UAV-based ~~V~~very high-resolution point cloud, ~~terrain~~ digital surface model and orthomosaics~~surveys~~ of the Chã das Caldeiras lava fields (Fogo Island, Cape Verde)

Gonçalo Vieira[1], Carla Mora[1], Pedro Pina[2], Ricardo Ramalho[3,4,5,6], Rui Fernandes[7]

[1]Centre of Geographical Studies (CEG), IGOT, University of Lisbon, Lisbon, 1600-276 Lisboa, Portugal
[2]Centre of Natural Resources and Environment (CERENA), IST, University of Lisbon, Lisbon, 1049-001 Lisboa, Portugal
[3]Instituto Dom Luiz (IDL), Faculdade de Ciências, Universidade de Lisboa, 1749-016 Lisboa, Portugal
[4]Departamento de Geologia, Faculdade de Ciências, Universidade de Lisboa, 1749-016 Lisboa, Portugal
[5]School of Earth Sciences, University of Bristol, Wills Memorial Building, Queen's Road, Bristol BS8 1RJ, UK
[6]Lamont-Doherty Earth Observatory, Columbia University, Comer Geochemistry Building, PO Box 1000, Palisades, NY10964-8000, USA
[7]Instituto Dom Luiz (IDL), Universidade da Beira Interior, Covilhã, 6201-001 Covilhã, Portugal

Correspondence to: Gonçalo Vieira (vieira@igot.ulisboa.pt)

Abstract. Fogo in the Cape Verde archipelago off Western Africa is one of the most prominent and active ocean island volcanoes on Earth, posing an important hazard to both local populations and at a regional level. The last eruption took place between 23 November 2014 and 8 February 2015 in the Chã das Caldeiras area at an elevation close to 1,800 m above sea level. The eruptive episode gave origin to extensive lava flows that almost fully destroyed the settlements of Bangaeira, Portela and Ilhéu de Losna. ~~In~~ During December 2016 a survey of the Chã das Caldeiras area was conducted using a fixed-wing unmanned aerial vehicle (UAV) and Real-Time Kinematic (RTK) GNSS, with the objective of improving the ~~mapping~~ terrain models and visible imagery ~~accuracy~~ derived from satellite platforms~~,improving~~ from a ~~metric~~ to decimetric resolution and accuracy ~~in topography~~in the digital surface model~~,~~. The main result is a~~n ultra~~ very-high resolution and quality 3D point cloud with a Root Mean Square Error of 0.08 m in X, 0.11 m in Y and 0.12 m in Z, which fully ~~provides~~ covers the most recent lava flows~~unprecedented accuracy~~. The survey ~~covers~~comprises an area of 23.~~-~~9 km^2 and used 2909 calibrated images with an average ground sampling distance of 7.2 cm. The dense point cloud, ~~A d~~digital surface models and ~~an~~ orthomosaics with 25 and 10 cm resolution, a ~~are provided, together with~~ 50 cm spaced elevation contour shapefile,~~s with an equidistance of 50 cm and~~ a 3D texture mesh ~~for visualization purposes~~, as well as ~~.~~ the full aerial survey dataset are provided. The delineation of the 2014-15 lava flows ~~shows~~ covers an area of 4.53 km^2 ~~by lava~~, which is smaller but more accurate than the previous estimates from 4.8 to 4.97 km^2. The difference in the calculated area, when compared to previously reported values, is due to a more detailed mapping of the flow geometry and to the exclusion of the areas corresponding to kīpukas (outcrops surrounded by lava flows). Our study provides a~~n ultra~~ very high-resolution dataset of the areas affected by Fogo's latest eruption ~~– crucial for local planning –~~ and ~~provides~~ is a case study supporting ~~to determine~~ the advantageous uses of ~~ultra high-resolution~~ UAV aerial photography surveys in disaster-prone areas. This dataset ~~is~~provides accurate baseline data for future eruptions, allowing for different applications in ~~e~~Earth system sciences,

Formatou: Português (Portugal)

Formatou: Superior à linha

Formatou: Superior à linha

Formatou: Superior à linha

such as hydrology, ecology, spatial ~~modelling~~modelling, ~~orand~~as well as to planning. The dataset is available for download at https://doi.org/10.5281/zenodo.471852~~10.5281/zenodo.4667709~~~~10.5281/zenodo.4035038 (Vieira et al., 2020)~~.

1. Introduction

Detailed knowledge o~~n~~f volcanic eruptions, their products, evolution and impacts is of paramount importance for ~~volcanic~~ hazard assessment~~s~~ and ~~to~~ for advanc~~e~~inge our capability to forecast the likely behaviour of future eruptions. Volcanic eruptions may ~~incur~~ result in considerable loss of life and lasting damage to infrastructures, particularly on ~~S~~small ~~D~~developing ~~I~~island ~~S~~states like Cape Verde, where ~~volcanic eruptions~~they are likely to have disproportionate impacts, on account of the~~ir~~ more limited resources and geographical isolation (Komorowski et al., 2016). ~~Furthermore, a~~A study commissioned by the United Nations Development Program in Cape Verde stresses that an improvement in the assessment of hazards on the island of Fogo can only be achieved from a detailed analysis and the modelling of the lava flow~~s~~ (Fonseca et al., 2014). ~~A study commissioned by the United Nations Development Program in Cape Verde stresses that an improvement in the assessment of hazards on the island of Fogo can only be achieved from a detailed analysis and the modelling of the lava flow (Fonseca et al., 2014). T~~Accordingly, ~~solid and~~ realistic volcanic hazard assessments in such areas, ~~more than in any other settings,~~ greatly benefit from very~~-~~ high~~-~~ resolution datasets from which detailed volcanological, geophysical~~,~~ and environmental parameters can be inferred. In particular, very high-resolution digital terrain datasets of recently erupted lava~~-~~ ~~flow~~ fields~~,~~ may ~~provide rapidly produced topographical datasets that can~~ also be used to plan mitigation and reconstruction strategies~~, as well as the opening of vital new transport and communication infrastructures~~. They also allow for very high- resolution mapping of small-scale features, such as pressure ridges, fractures, lava types, kīpukas (i.e. small 'islands' - interior elevations surrounded by lava), etc. that contribute to process-studies and to a better understanding of the eruption and post-eruption landscape dynamics. The usefulness of such datasets is greatly enhanced when these ~~datasets~~ are freely available to governmental agencies, decision-making ~~bodies~~bodies, and the scientific community alike.

Digital elevation models (DEM) and the dissemination of Geographical Information Systems have changed the way the terrain is characterized, analysed, monitored and modelled, especially since the 1990s. DEMs have been produced from dense collections of topographic points, manned aircraft photogrammetry, digitizing of topographic maps (Stevens et al., 1999), satellite remote sensing (Baldi et al., 2002; Kerle, 2002; Diefenbach et al., 2013), light detection and ranging (LiDAR; Mouginis-Mark and Garbeil, 2005; Mazzarini et al., 2007; Favalli et al., 2009; Fornaciai et al., 2010) and~~,~~ radar interferometry (InSAR; Rowland et al., 1999; Poland, 2014). The technological developments and decreasing cost of unmanned aerial vehicles (UAV), accompanied by the development of advanced photogrammetry algorithms involving image matching and structure from motion (SfM) and computing power, originated a significant methodological leap, that greatly affected practices in Earth surface sciences (James et al., 2019). The recent development of real-time kinematic (RTK) Global Navigation Satellite System (GNSS) UAVs results in even faster in-situ workflows and in the production of

Formatada: Avanço: Primeira linha: 1,27 cm

highly accurate models. As a result, very accurate and high quality DEMs and orthomosaics became increasingly used in the Earth sciences, allowing for centimetric to decimetric resolution even over large areas (Favalli et al 2018).

Several recent reviews have been produced showing the applicability of UAV based topographical surveys in volcanological research.~~.~~ Dering et al. (2019) present a review on UAV-based photogrammetry for mapping dykes in very high-resolution, emphasising on best-practices. A recent summary about the use of small UAV for collecting immediate and real-time aerial data in volcanic environments during and after an eruption is provided by Jordan (2019), highlighting its advantages for mapping, sample collection, thermal imaging, magnetic surveys, slope stability studies and as platforms for carrying outgassing measurement sensors. James et al. (2020) present a ~~very~~ complete review of applications of UAV to volcanology.

Unfortunately, despite the increasing use of UAV-based surveys, most of them remain inaccessible, lacking on their potential for reuse and for wider applications. Hence, making high quality datasets available as open access is essential. In line with this and with the needs indicated above, in ~~line with this vision, in this paper we report and make available a recently acquired very high-resolution digital surface model and orthomosaic of the lava flow flow~~ field created during~~of the 2014-15 eruption of Fogo volcano in Cape Verde.~~the remit of the project FIRE (Fogo Island volcano: multidisciplinary Research on 2014/15 Eruption), an extensive aerial photography survey using a survey-grade unmanned aerial vehicle ~~(UAV)~~ was conducted in the Chã das Caldeiras area in Fogo Island (Cape Verde) in December 2016. The main objectives were generating a very high-resolution (< 50 cm) digital surface model (DSM) and orthomosaic of the lava field to be used as baseline data for assessment of the eruption impacts, support to geological mapping and studies of the lava flow field, as well as for modelling lava flow dynamics. The data presented here is the result of that campaign and is the most detailed and updated terrain survey of the area. It comprises very-high resolution DSMs and digital orthomosaics (10 and 25 cm), accompanied by the dense point cloud, the 2014-15 lava flow delineation, as well as by the full survey data set.

2. The study area

The island of Fogo is one of ten islands of Cape Verde, an archipelago located off the west African coast, about 600 km from Senegal (Fig. 1). Fogo is one of the most prominent and active ocean island volcanoes on Earth, posing an important hazard to local populations and at a regional level (Day et al., 1999; Heleno da Silva et al., 1999; Ramalho et al., 2015; Eisele et al., 2015; Jenkins et al. 2017). Crucially, Fogo is the site of recurring volcanic activity, with a record of at least 27 historical eruptions since the island was discovered in the mid-fifteenth century, yielding a mean recurrence interval between eruptions of about 20 years, with individual intervals ranging from 1 to 94 years (Ribeiro, 1954; Torres et al., 1998; Day et al., 1999; Mata et al., 2017). The latest events occurred in 1995 and in 2014-15, both extruding extensive lava fields at the Chã das Caldeiras, a summit depression lying at approximately 1800 m altitude (Fig. 1). The settlements of Bangaeira, Portela and Ilhéu de Losna located in Chã das Caldeiras were almost fully destroyed in the 2014-15 eruption ~~(Fig. 1)~~. Fortunately, there were no casualties.

Formatada: Avanço: Primeira linha: 1,27 cm

Cape Verde islands are regarded as the type-example of a volcanic archipelago formed in a stationary plate environment relative to its hotspot, which probably explains the arcuate distribution of its islands (Fig. 1, Burke & Wilson 1972; Lodge and Helffrich, 2006; Ramalho et al., 2010a, 2010b, 2010c; Ramalho, 2011). In more detail, this arcuate geometry is defined by two island chains: a "northern", from São Nicolau to Santo Antão, and a "eastern-to-southern", from Sal to Brava. There is no evident hotspot track but there is a morphological suggestion of an age progression in the "eastern-to-southern chain", from east (oldest islands) to west (youngest islands) (see Ramalho, 2011). Fogo is located close to the southern terminus of this latter chain and is the only island in the archipelago with historical (i.e. last 500 years) eruptions (Bebiano, 1932; Ribeiro, 1954; Machado, 1965; Day et al., 1999; Faria and Fonseca, 2014).

~~The island of Fogo is one of ten islands of Cape Verde, an archipelago located off the west African coast, about 600 km from Senegal. Fogo in the Cape Verde Archipelago off Western Africa is one of the most prominent and active ocean island volcanoes on Earth, posing an important hazard to both local populations and at a regional level (Day et al., 1999; Heleno da Silva et al., 1999; Ramalho et al., 2015; Eisele et al., 2015; Jenkins et al. 2017). Crucially, Fogo is the site of recurring volcanic activity, with a record of at least 27 historical eruptions since the island was discovered in the mid-fifteenth century, yielding a mean recurrence interval between eruptions of approximately 19.8 years, with individual intervals ranging from 1 to 94 years (Ribeiro, 1954; Torres et al., 1998; Day et al., 1999; Mata et al., 2017). The latest events occurred in 1995 and in 2014-15, both of which extruded~~ extruding ~~extensive lava flow fields at the Chã das Caldeiras, a summit depression lying at an elevation of approximately 1800 m above mean sea level. Effectively, t~~The settlements of Bangaeira, Portela and Ilhéu de Losna ~~located in Chã das Caldeiras were almost fully destroyed in the 2014-15 eruption (Fig. 1). With a population of about 1200 inhabitants prior to the eruption, the local economy was based in agriculture (mainly wine and fruit orchards), grazing, and tourism. Fortunately, there were no casualties.~~

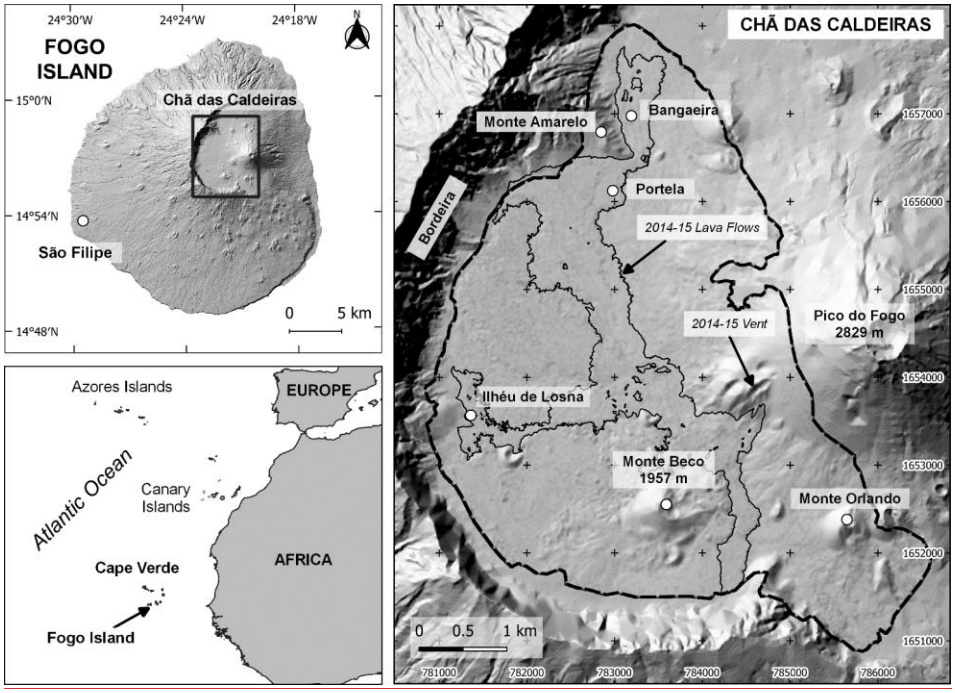

Figure 1 – Location of the Chã das Caldeiras and of the surveyed area (dashedblack line) in Fogo Island (Cape Verde). The 2014-15 lavae flows are limited by a thin black line. Shaded relief derived from the DEMFI (2010) 5 m DEM.

The latest eruption started on the 23rd November 2014 and lasted until the 8th February 2015, with magma being erupted from a 700 m-long NE–SW trending eruptive fissure located on ¬the SE flank of the previous 1995 crater row, on the SW flank of Pico do Fogo (Vieira et al., 2016; Mata et al., 2017). Reportedly, the eruption started with vigorous fire-fountain activity, which quickly evolved to a more explosive strombolian style, forming a crater row roughly parallel to the 1995 fissure. Later, the eruption was characterized by simultaneous or alternating hawaiian, strombolian and vulcanian eruptive styles (from the different craters of the fissure) lasting for several days, and by an almost constant emission of lava flows from the lowermost terminus of the vent (Mata et al., 2017). These formed two initial thick 'a'ā flow lobes: the first advanced towards the southwest and eventually stalled after 1.7 km, at the foot of the caldera wall; the second progressed

intermittently 3 km to the northeast, towards the village of Portela, razing a large portion of this settlement (Mata et al. 2017; Jenkins et al., 2017). During the later stages of the eruption, however, this flow lobe was reactivated, producing more fluid ‘a'ā and pāhoehoe breakouts to the west and north, the latter of which destroyed most of what was left of the Portela settlement and descended to the village of Bangaeira, causing widespread destruction there (Mata et al. 2017; Jenkins et al., 2017). The resulting lava flow field affected an area of ci. 4.8 km^2, with extruded volumes estimated at ~45 × 10^6 m^3 (Bagnardi et al., 2016; Richter et al., 2016; Cappello et al. 2016).

Remote sensing techniques have been used by several authors to study the Fogo eruption of 2014-15. Capello et al. (2016) used the HOTSAT satellite volcano thermal monitoring system for the analysis of Moderate Resolution Imaging Spectroradiometer (MODIS) and Spinning Enhanced Visible and Infrared Imager (SEVIRI) data for to determine the location of the hotspot, lava thermal flux, and effusion rate estimation. To forecast model lava flow hazards during the 2014-15 Fogo eruption they used the MAGFLOW model. Validation of numerical simulations was done using Landsat 8 OLI and EO-1 ALI images and field observations. Bargnardi et al. (2016) used very high-resolution tri-stereo optical imagery acquired by the Pleiades-1 satellite constellation and generated a 1 m resolution digital elevation model (DEM) of the Fogo Volcano. From the Pleiades-1 post-eruption topography they subtracted the heights from a pre-eruption DEM, that was obtained using spaceborne synthetic aperture radar (SAR) data from the TanDEM-X mission. To measure the subsidence of the lava flow field, they used Sentinel-1 for interferometry. Height differences between the post-eruptive Pleiades-1 DEM and the pre-eruptive topography from TanDEM-X showuggest a lava volume of 45.83 ± 0.02 × 10^6 m^3, emplaced over an area of 4.8 km^2 at a mean rate of 6.8 m^3/s. Richter et al. (2016) did lava flow simulations based on field topographic mapping and satellite remote sensing analysis. They produced a topographic model of the 2014-15 lava flows from combined Terrestrial Laser Scanner (TLS) and photogrammetric data. The pre-eruptive DEM used was 5 m/pixel and was generated from the contours based on photogrammetric data. They estimated a lava flow volume of 43.7 ± 5.2 x 10^6 m^3. TerraSAR-X imagery was used to access the lava flow model performance. The authors point outhighlight the need of havingfor up-to-date topographic information because lava flow hazards change as a result of topographicy modifications.

More recently, Bignami et al. (2020) used a combined method of 21 images from Sentinel-1, COSMO-SkyMed, Landsat 8, and Earth-Observing-1 missions from November 2014 to January 2015, to retrieve lava flow patterns. They applied an automatic change detection technique for estimating the lava field and its temporal evolution, combining the SAR intensity and the interferometric SAR coherence. Results showed a SW-NE oriented dyke, located inside Chã das Caldeiras, SW of the Pico do Fogo, as reported by Gonzalez et al. (2015). The area coverage of the lava flow obtained by visual analysis (L8 and EO-1) was estimated at 4.97 km^2 as in Cappello et al. (2016), very close to the 4.8 km^2 estimated by Bagnardi et al. (2016), and the 4.85 km^2 estimated using Terrestrial Laser Scanner (TLS) combined with structure from motion data by Richter et al. (2016).

Several papers have been published on the latest eruption of the Fogo volcano, e.g., focusing on the variation of land surface temperatures during the eruption (Vieira et al., 2016), on lava geochemistry and small-scale mantle heterogeneity (Mata et al., 2017), mineralogy and geochemistry of incrustations (Silva et al., 2019), conduit dynamics and surface deformation

(Gonzalez et al. 2015), on lava flow mapping and volume estimates (Bargnardi et al. 2016; Bignami et al., 2020), and lava flow hazards (Richter et al., 2016; Cappello et al. 2016; Jenkins et al., 2017).

In the remit of the project FIRE (Fogo Island volcano: multidisciplinary Research on 2014/15 Eruption, funded by FCT-Portugal), an extensive aerial photography survey using a survey-grade unmanned aerial vehicle (UAV) was conducted in December 2016. The objectives were with the purpose of generating a very high resolution (< 50 cm) digital elevation model (DEM) and orthomosaic of the lava field to be used as baseline data for assessment of the eruption impacts, support to geological mapping and studies of the lava flow field, as well as for modelling lava flow dynamics. A study commissioned by the United Nations Development Program in Cape Verde stresses that an improvement in the assessment of hazards on the island of Fogo can only be achieved from a detailed analysis and the modelling of the lava flow (Fonseca et al., 2014). The data presented here is the result of that campaign and is the most detailed and updated survey of the area, with an ultra-high resolution digital surface model (DSM) that is essentially a DEM in most of the area due to the overall lack of vegetation and scarce number of buildings, and a digital orthomosaic.

2. Application of UAVs to volcanic areas

Digital elevation models and the dissemination of Geographical Information Systems have changed the way the terrain is characterized, analysed, monitored and modelled, especially since the 1990's. DEMs have been produced from dense collections of topographical points, manned aircraft photogrammetry, digitizing of topographic maps (Stevens et al., 1999), satellite remote sensing (Baldi et al., 2002; Kerle, 2002; Diefenbach et al., 2013), light detection and ranging - (LiDAR; (Mouginis-Mark and Garbeil, 2005; Mazzarini et al., 2007; Favalli et al., 2009; Fornaciai et al., 2010), radar interferometry (InSAR;) (Rowland et al., 1999; Poland, 2014). Since the mid 2010's, with tThe technological developments and decreasing cost of unmanned aerial vehicles, accompanied by the development of advanced photogrammetry algorithms involving image matching and structure from motion (SfM) software and computing power, a revolution took placeoriginated a significant methodological leap, that greatly affected practices in Earth surface sciences (James et al., 2019). The recent development of real-time kinematic (RTK) Global Navigation Satellite System (GNSS) UAVs results in even faster in-situ workflows and in the production of highly accurate models. As a result, Vvery accurate and high quality DEMs and orthomosaics became increasing availablely used in the Earth sciences, leading to the possibility to easily achieveallowing for centimetric to decimetric resolution, even in over large areas. The number of UAV-based surveys have been increasing steadily but many of them stay stored in the producers or client computers and are not of open-access. (Favalli et al 2018). Unfortunately, despite the increasing use of UAV-based surveys, most of them remain inaccessible, lacking on their potential for reuse and for wider applications. Hence, making high quality datasets available as open access is essential.

UAVs have had various applications, such as for wildlife recognition (e.g. Christiansen et al., 2014; Wang et al., 2019), agriculture (e.g. Hassan-Esfahani et al., 2015, Kattenborn et al. 2014; Hasseler and Baysal-Gurel, 2019), urban and civil engineering (Westfeld et al., 2015), archaeology (Campana 2017; Risbøl and Gustavsen 2018), coastal dynamics (Chikhradze et al 2015; Brunier et al 2016; Turner et al 2017; Long et al 2016), climatology (Lindgren et al 2015;

Formatada: Título 1

Bühler et al 2016), geomorphology (Lucieer, et al 2014; Dabski et al. 2020), vegetation in Polar regions (Mora et al 2015, Miranda et al 2020), glacier monitoring (Benoit et al 2019; Jouvet et al 2020) or for monitoring volcanic systems (Chio and Lin, 2017; Thiele et al., 2017).

Applications of UAV surveys to research in the Earth and Atmosphere sciences are relatively recent, having begun to emerge with greater expression frequency from 2014 (Colomina and Molina 2014; Pajares 2015). Since then the number of publications has grown rapidly and spread across research fields, developing into a technique allowing fast and low-cost access to high spatial resolution data (Gomez and Purdie, 2016). The significanthigh versatility of UAV applications, in addition to the added value of accessing otherwise rough, remote terrains and possibilities of surveying even rough terrains of difficult access, such as the situation of such a volcanic eruption sites - volcanic eruptions, make UAVsmake them a powerful tool to for acquiringe real-time or near-real-time data on processes that often cannot be observed by the naked eye (Di Felice et al. 2018). Hence UAVs are increasingly used in situations of risk where it is essential to undertake rapid terrain recognitionto make the rapid terrain recognition following natural disasters (Gomez and Purdie 2016).

Software and computing power have evolved very fast in last decade and the application of advanced photogrammetry algorithms involving image matching and structure from motion started to allow facilitated production of high-quality digital surface models and orthophoto maps. The collection of accurate GNSS ground control points allows to generate these products with centimetre resolution and accuracy (Favalli et al 2018). The recent development of RTK UAVs allows for even faster workflows in the terrain and to produce highly accurate models.

Photogrammetry techniques haves been widely applied to study detailed changes in the morphology and structures of volcanos, like Mount St. Helens, the Colima and the Merapi (Major et al., 2009; Walter et al., 2013; Salzer et al., 2016). Optical and thermal cameras transported on UAVs have been used for identifying meter to sub-meter topography changes and for the detection of thermal anomalies (Nakano et al., 2014; Thiele et al., 2017; Nakano et al., 2014; Müller et al., 2017; Amici et al., 2013; Di Felice et al 2018). In addition, specific payload sensors are being used for measuring volcanic gas fluxes (McGonigle et al., 2008; Liu et al. 2019; de Moor et al., 2019), gas sampling (Mori et al., 2016; Rüdiger et al., 2018; Stix et al., 2018) and sediment sampling (Yajima et al., 2014).

Various sStudies have shown demonstrated the potential of UAV-based photogrammetric surveying in volcanic terrains, . These show the potential of the survey produced at Fogo, not only for characterizing post-eruption changes, but also for providing baseline data for analysing the dynamics evolution of the lava flow fields upon during cooling, or the soil erosion and even human reoccupation of the area. As examples of UAV-based mapping, aAt the Nishinoshima Volcano, Nakano et al. (2014) have acquired visible imagery to produce 3D maps allowing to monitor the evolution of the volcano. Darmawan et al. (2018) studied morphological and structural changes from 2012 to 2015 at the Merapi lava dome having identified the locations of steam-driven explosions. Felice et al. (2018) surveyed the erupting crater of Indonesian Lusi mud eruption as its was spewing erupting boiling mud, water, aqueous vapour, CO_2, and CH_4. Favalli et al. (2018) generated a high spatial resolution digital terrain model and orthomosaic of Mount Etna's January–February 1974 lava flow field, allowing the analysis of the morphology of sub-meter features, such as folds, blocks, and cracks, over kilometre-scale areas. The 3-cm orthomosaic allowed the analysis of centimetre-scale grain size distribution of the lava surface. Müller et al. (2017) studied the 2014-15 fissure eruptions of the Holuhraun to investigate the link between magma dikes at depth and the association with elastic and inelastic surface deformation. Turner et al (2017) during the 2014–15 Pāhoa crisis, used a UAV to monitor the front of a slowly advancing pāhoehoe lava flow. UAV surveys allowed Bonali et al. (2019) to study volcano-tectonics and tectonic features in an active Icelandic rift with unprecedent detail in extended areas in a much faster way and much

lesser funds with respect to traditional field activity. One of the first UAV surveys during an ongoing eruption was performed by De Beni et al. (2019) in the 27 February–02 March 2017 event of Mt. Etna, which allowed improving the monitoring quality of the lava flow in terms of timeliness and detail. The independent acquisition of both visible and thermal infrared imagery by a pair of UAV in Stromboli allowed Wakeford et al. (2019) to build a 3D photogrammetric model of an active volcano. Dering et al. (2019) present a review on UAV-based photogrammetry for mapping dykes in very high-resolution, emphasising on best-practices. Finally, a recent summary about the use of small UAV for collecting immediate and real-time aerial data in volcanic environments during and after an eruption is provided by Jordan (2019), highlighting its advantages for mapping, sample collection, thermal imaging, magnetic surveys, slope stability studies, and also as platforms for carrying outgassing measurement sensors.

3. The study area and the volcanic activity of 2014-15

The island of Fogo is one of ten islands of Cape Verde, an archipelago located off the west African coast, about 600 km from Senegal. The Cape Verdes islands are regarded as the type-example of a volcanic archipelago formed in a stationary plate environment relatively to its hotspot, which probably explains the arcuate distribution of its islands (Fig. 1, Burke & Wilson 1972; Lodge and Helffrich, 2006; Ramalho et al., 2010a, 2010b, 2010c; Ramalho, 2011). In more detail, this arcuate geometry is defined by two island chains: a "northern", from São Nicolau to Santo Antão, and a "eastern-to-southern", from Sal to Brava. There is no evident hotspot track but there is a morphological suggestion of an age progression in the "eastern-to-southern chain", from east (oldest islands) to west (youngest islands), which is also supported by ages of the oldest exposed lithologies (see Ramalho, 2011). Fogo is located close to the southern terminus of this latter chain and is the only island in the archipelago with historical (i.e. last 500 years) eruptions (Bebiano, 1932; Ribeiro, 1954; Machado, 1965; Day et al., 1999; Faria and Fonseca, 2014).

Fogo is a large ocean island volcano showing a conical shape with a diameter of about 30 km (at sea level) and rising to an elevation of 2829 m, approximately 7 km above the surrounding seafloor. Structurally, the island is a compound volcano, featuring a "somma-vesuvio" association, with a younger stratovolcano – Pico do Fogo – rising from the central depression – Chã das Caldeiras – of an older collapsed volcano, sometimes referred as Monte Amarelo (Ribeiro, 1954; Day et al., 1999). This depression, however, is open to the east, being limited bounded in the remaining three sides by a horseshoe shaped steep rock wall, over 1,000 m high, called Bordeira (Fig. 1). This morphology, in turn, is either interpreted as a gravitational collapse headwall (Day et al., 1999; Paris et al., 2011) or as volcanic caldera walls, whose eastern portion later experienced a gravitational flank failure (Torres et al., 1998; Brum da Silveira et al., 1997a, 1997b; Madeira et al., 2008). Notwithstanding the different interpretations for the origins of this summit depression, it is clear that the opening to the east resulted from a massive flank failure of the flank of the volcano. Effectively, marine geophysical surveys undertaken off the coast of Fogo revealed the presence of voluminous submarine debris avalanche deposits extending offshore into the channel between Fogo and Santiago, and into the seafloor south and north of these islands, thus attesting to the occurrence of this collapse (Le Bas et al., 2007; Masson et al., 2008; Barrett et al., 2019b). Moreover, field evidence attesting to the impact of a megatsunami triggered by Fogo's flank failure has been documented in the neighbouring islands of Santiago (Paris et al., 2011, 2018;

Ramalho et al., 2015) and Maio (Madeira et al., 2020), confirming the catastrophic nature of the collapse and suggesting a 65-84 ka age for this event.

Pico do Fogo, currently the highest point in the island ~~(2829 m in elevation).~~ is a large and roughly symmetrical strato-cone that grew on top of the collapse scar, partially infilling this feature (Ribeiro, 1954; Torres et al., 1997; Brum da Silveira et al., 1997a, 1997b; Day et al., 1999). ~~The sheer volume of this volcanic edifice is a testimony to the vigorous eruptive activity taking place at Fogo Island. There have been suggestions that Pico do Fogo experienced summit eruptions as late as the 18th century (Day et al., 1999), however this seems to be contradicsted by the stratigraphic sequence at the summit, which exhibits mostly altered volcanic successions.~~ ~~Effectively,~~ hHistorical records suggest that all historic eruptions were extruded from adventitious vents locatedlised at the base and lower flanks of Pico do Fogo, or at Chã das Caldeiras and the eastern flank of the island, in the periphery of this strato-cone (Ribeiro, 1954; Torres et al., 1997; Brum da Silveira et al., 1997a, 1997b). This is the case of the 1951, 1995, and 2014-15 eruptions, which had ~~which~~ vents ~~were~~ located in the ~~NW~~northwestern, ~~SW~~ southwestern and ~~S~~ southern flanks of Pico do Fogo, close to its base at Chã das Caldeiras.

Chã das Caldeiras (Fig. 2) is thus a lava-infilled, high-altitude summit depression, which resulted from the gradual accumulation and ponding of lava flows (and pyroclasts) erupted from Pico do Fogo and its adventitious/satellite cones, against the vertical walls of Bordeira. Morphologically, the Chã can be divided in two large semi-circular sectors: a southern, larger, with approximately 3 km of radius, and with an elevation of 1780 m, and a northern, with a shorter radius of approximately 1 km, and with a mean elevation of 1650 m. These two sectors, which are roughly separated by the prominent Monte Amarelo spur, have been interpreted as two coalescent volcanic calderas by Torres et al. (1997), Brum da Silveira et al. (1997a, 1997b), and Madeira et al. (2008). Chã das Caldeiras is ~~a~~ generally a flat landscape, punctuated by a few volcanic cones and extensively covered by ‘a'ā and pāhoehoe lava flows and ash and lapilli deposits, which make it a ~~very irregular in detail~~rough and ~~a~~ challenging terrain for mapping. In particular, the extensive ‘a'ā lava flow lobes of the 2014-15, 1995 and 1951 eruptions covered large portions of Chã, resulting in ~~large~~ wide swaths of virtually inaccessible rocky surfaces, given their ~~extreme~~ roughness. Hummocky landscapes also exist, generally corresponding to older ‘a'ā lava flow fields with ~~scattered~~ large, scattered, rafted blocks of spatter sequences ~~in~~ on its surface (resulting from the gravitational collapse of strombolian cones and subsequent transport by lava flows), which are now partially buried under a blanket of lapilli and ash that smoothed the surface. A good example of such surfaces can be found to the east, and particularly to the west of the Monte Beco cone, being genetically associated to this vent. The foot and slopes of Pico do Fogo, in contrast, are extensively covered by a thick blanket of lapilli and ash, ~~conferring~~ resulting in a very smooth and uniform conical surface. Despite this cover, fanned leveed channel~~led~~ morphologies can also be recognized at the foot of Pico do Fogo, corresponding to buried lava flow fans and alluvial fans. Overall, vegetation is scarce and is mostly confined to the surfaces of talus accumulated at the foot of Bordeira, where a thin soil exists, or to some scattered vineyards along ~~some~~ ash-covered slopes.

Comentado [GV1]: R3: repetition

Comentado [GV2R1]: OK. deleted

Figure 2 – The Chã das Caldeiras and Pico do Fogo during the 2014-15 eruption. View towards the southeast with the 'a'ā lava flows of 2014-15 in the foreground, evidencing a very irregular and inaccessible surface. The active volcanic vent is visible in the SW flank of the Pico do Fogo.

Human settlement at Chã das Caldeiras started towards the end of the 19th century (Ribeiro, 1954). The area is cooler and more humid than the rest of the island, with frequent fog condensation and occasional frosts, providing ideal conditions for the planting of orchards and vineyards. Attracted by the prospect of a more prosperous agriculture, people gradually settled the Chã, mostly in the vicinities of Monte Amarelo. There, springs and ephemeral stream flow from the larger canyons draining Bordeira allowed easier access to water. Here they established the settlements of Portela, Boca Fonte, and later Bangaeira, which slowly and gradually grew until the 1995 eruption. Then, Boca Fonte was all but destroyed and the main access road to these settlements was blocked by the advancing flows (Jenkins et al., 2016). After the 1995 eruption, the prospect of an additional income provided by a burgeoning wine industry and the rapidly growing flow of tourists that came to see the volcano, fuelled the rapid growth of Portela and Bangaeira, with population reaching as much as ~1500 resident inhabitants by 2014 (Fonseca et al., 2014; Jenkins et al., 2016). The 2014/2015 eruption had a profound impact in these villages, as the advancing lava flows either razed or buried up to 90% of the existing buildings and covered large swaths of agricultural land. Gradually, however, reconstruction is taking place, both through new constructions over the recent lava flows, and by the painstaking reclamation of lava-buried but structurally intact buildings.

3. The volcanic activity of 2014-15 and previous digital elevation models

The latest eruption in Fogo started on the 23rd November 2014 and lasted until the 8th February 2015, with magma erupting from a 700 m-long NE–SW trending fissure on the SE flank of the 1995 crater, on the SW flank of Pico do Fogo (Vieira et al., 2016; Mata et al., 2017). Reportedly, the eruption started with vigorous fire-fountain activity, which quickly evolved to a more explosive strombolian style, forming a crater row roughly parallel to the 1995 fissure. Later, the eruption was characterized by simultaneous or alternating Hawaiian, strombolian and vulcanian eruptive styles (from the different craters of the fissure) lasting for several days, and by an almost constant emission of lava from the lowermost terminus of the vent (Mata et al., 2017). These formed two initial thick ‘a'ā flow lobes: the first advanced towards the southwest and eventually stalled after 1.7 km, at the foot of the caldera wall; the second progressed intermittently 3 km to the northeast, towards the village of Portela, razing a large portion of the settlement (Mata et al. 2017; Jenkins et al., 2017). During the later stages of the eruption, this flow lobe was reactivated, producing more fluid ‘a'ā and pāhoehoe breakouts to the west and north, the latter of which destroyed most of what was left of the Portela settlement and descended to the village of Bangaeira, causing widespread destruction there (Mata et al. 2017; Jenkins et al., 2017). ~~The resulting lava flow field affected an area of ca. 4.8 km^2 (Bagnardi et al., 2016; Richter et al., 2016; Cappello et al. 2016).~~

Remote sensing techniques have been used by several authors to study the Fogo eruption of 2014-15. Capello et al. (2016) used the HOTSAT satellite volcano thermal monitoring system for the analysis of Moderate Resolution Imaging Spectroradiometer (MODIS) and Spinning Enhanced Visible and Infrared Imager (SEVIRI) data to determine the location of the hotspot, lava thermal flux, and effusion rate. Validation of numerical simulations was done using Landsat 8 OLI and EO-1 ALI images and field observations.

Bagnardi et al. (2016) used very high-resolution tri-stereo optical imagery acquired by the Pleiades-1 satellite constellation and generated a 1 m resolution ~~digital elevation model (~~DEM~~)~~. The model accuracy was calculated from differential GPS solution from 19 ground control points. The mean offsets obtained were -7.6 m (easting) and -1.3 m (northing), with standard deviations of respectively, 0.4 and 0.3 m. The mean height difference (MHD) was -2.84 and the standard deviation (STD) was 0.51 m. The authors also generated a DEMs using spaceborne synthetic aperture radar (SAR) data from the TanDEM-X mission, generating 5 m/pixel model with a MHD of -0.1 m and STD of 1.12 m. They have also evaluated coarser resolution public DEMs against the GCPs: the SRTM (30 m) shows a MHD of -3.5 m and a STD of 3.64 m, and the ASTER-GDEM (30 m) resulted in a MHD of -8.56 m and in a STD of 5.74 m. From the Pleiades-1 post-eruption topography they subtracted the heights from ~~a~~the pre-eruption DEM ~~that was obtained using spaceborne synthetic aperture radar (SAR) data from the TanDEM-X mission~~. ~~To measure the subsidence of the lava flow field, they used Sentinel-1 for interferometry.~~

Height differences ~~suggest~~indicate a lava volume of 45.83 ± 0.02 × 10^6 m^3, emplaced over an area of 4.8 km^2 at a mean rate of 6.8 m^3/s.

Formatada: Avanço: Primeira linha: 1,27 cm

Richter et al. (2016) did lava flow simulations based on field topographic mapping and satellite remote sensing analysis. They produced a topographic model of the 2014-15 lava flows from combined Terrestrial Laser Scanner (TLS) and photogrammetric data obtained from 77 oblique images obtained with dSLR 15.1-megapixel Canon EOS Rebel cameras. The resulting DEM represents the conditions at 16 January 2015 and shows a 5 m resolution and a RMSE of 1.08 m in relation to a pre~~The pre~~-eruptive 5 m/pixel DEM ~~used was~~ produced by GRAFCAN in a mapping campaign in 2003-04. The comparison of both ~~5 m/pixel and was generated from the contours based on photogrammetric data,~~ allow~~ed~~ing to estimate a lava volume of 43.7 ± 5.2 x 10^6 m^3. ~~-~~TerraSAR-X imagery was used to assess the lava flow model performance. The authors highlight the need for up-to-date topographic information because lava flow hazards change, as a result of topographic modifications.

More recently, Bignami et al. (2020) combined 21 images from Sentinel-1, COSMO-SkyMed, Landsat 8, and Earth-Observing-1 missions from November 2014 to January 2015 to retrieve lava flow patterns. They applied an automatic change detection technique for estimating the lava field and its temporal evolution, combining the SAR intensity and the interferometric SAR coherence. The area coverage of the lava flow obtained by visual analysis (L8 and EO-1) was estimated at 4.97 km^2 as in Cappello et al. (2016), very close to the 4.8 km^2 estimated by Bagnardi et al. (2016), and the 4.85 km^2 estimated using Terrestrial Laser Scanner (TLS) combined with structure from motion data by Richter et al. (2016).

The DEMs produced previously show spatial resolution of 1 to 5 m and metric accuracies. In this paper we present and make public a new data set that ~~presented here~~ fills the gap ~~in knowledge~~ from the metric to the decimetric scale and ~~identified by several authors and stakeholders and~~ provides a new tool for multiple applications in various fields of the Earth and environmental sciences and planning.

~~Figure 2 – The Chã das Caldeiras and Pico do Fogo during the 2014-15 eruption. View towards the southeast with the 'a'ā lava flows of 2014-15 in the foreground.~~

Formatada: Centrado

~~Human settlement at Chã das Caldeiras started towards the end of the 19th century (Ribeiro, 1954). Chã, as a high-altitude depression, is cooler and more humid than the rest of the island, with frequent fog condensation and occasional frosts, providing ideal conditions for the planting of orchards and vineyards. Attracted by the prospect of a more prosperous agriculture, people gradually settled the Chã, mostly in the vicinities of Monte Amarelo, where some water springs and enhanced but ephemeral stream flow (from the larger canyons draining Bordeira) allowed easier access to water. Here they established the settlements of Portela, Boca Fonte, and later Bangaeira, which slowly and gradually grew in size until the 1995 eruption, when Boca Fonte was all but destroyed and the main access road to these settlements was blocked by the advancing flows (the 1951 eruption, although of a higher magnitude, had a lower impact in these settlements; Jenkins et al., 2016). After the 1995 eruption, however, the prospect of an additional income provided by a burgeoning wine industry and the rapidly growing flow of tourists that came to see the volcano, fuelled the rapid growth of Portela and Bangaeira, with population reaching as much as ~1500 resident inhabitants by 2014 (Fonseca et al., 2014; Jenkins et al., 2016). The 2014/2015 eruption, in contrast, had a profound impact in these villages, given thatas the advancing lava flows either razed or buried up to 90% of the existing buildings, as well asand covered large swaths of the adjacent agricultural land. Gradually, however, reconstruction is taking place, either both through new constructions over the recent lava flows, or and by the painstaking reclamation of lava-buried but structurally intact buildings.~~

~~4~~3. Methods

~~4~~3.1 UAV Surveying

The survey of the Chã das Caldeiras area ~~was conducted~~took place from 12 to 16 December 2016 with a ~~field~~ team of 4 members.~~:~~ ~~T~~two ~~members focussed~~working on ~~conducting~~ the UAV flight operations~~s~~ and ~~the other~~ two on ~~the~~ collecting ground control points. The~~ise~~ ~~field~~ campaign was conducted ~~about~~ roughly 20 months after the end of the eruption of 2014-15, when the lava flows had already cooled substantially. At the time~~, but with the occupation~~, some of the few houses at the Chã das Caldeiras had been reoccupied~~existing at the Chã das Caldeiras~~, despite that being forbidden and ~~still~~ hazardous, mainly due to gas emissions. Hence, the ~~field~~ team stayed at the village of São Filipe and travelled daily to the survey area.~~ The expertise of the team on local conditions, geology and logistics and cooperation with the Cape Verde authorities, greatly facilitated the success of the mission.~~

The main ~~main~~ logistical ~~challenges~~issues were: ~~to overcome were~~ i. the weather, which in December frequently shows high winds and low visibility (clouds) in the Chã das Caldeiras, ii. finding good landing sites for the UAV, iii. coping with the 1000 m high vertical rock wall of the Bordeira and ~~with~~ its ~~possible~~ potential influence on the positioning and communications system of the UAV, and iv. collecting enough high-quality ground control points.

Formatada: Avanço: Primeira linha: 1,27 cm

~~The survey of the Chã das Caldeiras area was conducted from 12 to 16 December 2016 with a field team of 4 members. Two members focussed on conducting the UAV flights and the other two on the collecting ground control points. Communications among team members were done using VHF radios.~~

The weather during the campaign ~~was excellent with~~showed mostly clear skies and no wind in the first days, but deteriorated ~~deteriorated~~ towards the end ~~of the week~~, with low clouds ~~entering the survey area and~~ affecting ~~initially~~ the illumination conditions and ~~even~~ limiting the flights in the last two days (Table 1). ~~This has affected the quality of the orthomosaic, which shows illumination artefacts in the northern part of the Chã das Caldeiras.~~

The survey was conducted using a ~~professional survey-grade~~ fixed-wing UAV SenseFly eBee classic, w~~hich has~~ith ~~a structure of expanded polypropylene (EPP) foam, with carbon and composite parts. It has~~ a 96 cm wingspan and under 0.7 kg take-off weight~~, which when disassembled allows for lightweight packing~~. The model has an internal GPS, a pitot probe, barometer and ground distance sensor and~~This model~~ allows for ~~-~~flights with wind speeds up to 45 km/h, flight durations of up to 50 min and a radio link distance up to 3 km. Two cameras were used: a Canon Powershot G9X 16MP in the initial flights, which had a critical failure, and a backup Canon IXUS 127HS 12 MP, which was used subsequently (Table 1). Flight planning was done with emotion2, with flights at an average height of 190 m above the ground surface, resulting in an average ground sampling distance of c. 6-7 cm. The images were collected with a longitudinal overlap of 60% and a lateral overlap of 65%. This setup was a compromise between: i. the aim to map features below ci. 50 cm, ii. maintaining flights under 200 m height from the ground surface for better control, iii. the time available for the surveying, and iv.~~s well as~~ battery limitations of the UAV.

~~Take-off with the eBee is performed by hand, which facilitates selecting the location, but landing is done normally in fully automatic mode needing several tens of meters of approach area, and a smooth landing surface in order not to damage the EPP UAV body. This was a significant limitation to the survey, since the area of the Chã das Caldeiras is mostly covered by very rough lava surfaces, with scarce smooth ash and lapilli cover sites, which are normally far apart. Given these constraints, five sites allowing for good landing conditions were selected (Fig. 3): (i.) 14.93477º N, 24.35407º W, (ii.) 14.928092º N, 24.353165º W, (iii). 14.92339º N, 24.356605º W, (iv). 14.9334999º N, 24.3722831º W and, (v.) 14.962204º N, 24.3690256º W.~~

Table 1 – Synthesis of flight characteristics and photos excluded from the modelling due to lack of calibration or manually disabled in the pre-processing.

Flight nr	Date (2016)	Start time	Duration (min)	Area (km^2)	Weather	Camera	Nr of Photos	First and last photo ID (IMG)	Used	Uncalibrated images IDs (IMG)	Disabled images IDs (IMG)
1	12/12	14:58	20	0.99	Cloudfree	~~Canon~~ G9X	92	0425 - 0516	Yes	448, 470	425-428, 451-460, 513-516
2	12/12	15:21	29	1.21	Cloudfree	~~Canon~~	150	0517 - 0666	Yes		517-519, 542, 564-

Tabela Formatada

						G9X					568, 613-615, 639-642
3	12/12	15:52	28	1.44	Cloudfree	~~Canon~~ G9X	181	0667 - 0847	Yes		671, 683
4	12/12	16:43	33	0.37	Cloudfree	~~Canon~~ G9X	50	0849 - 0898	Yes		
5	13/12	11:04	25	1.52	Cloudfree	~~Canon~~ G9X	161	0900 - 1060	Yes		1053-1060
6	13/12	11:31	35	1.37	Cloudfree	~~Canon~~ G9X	181	1061 - 1241	Yes	1200, 1241	1113-1116, 1155
7	13/12	12:59	30	1.41	Cloudfree	~~Canon~~ G9X	166	1243 - 1408	Yes		1244-1260, 1352, 1406-1408
8	14/12	11:00	19	1.40	Cloudfree	~~Canon~~ IXUS	215	0146 - 365	Yes		
9	14/12	11:55	27	1.19	Cloudfree	~~Canon~~ IXUS	205	366 - 570	Yes		
10	14/12	12:33	31	1.35	Cloudfree	~~Canon~~ IXUS	216	0571 - 0786	Yes	786	
11	14/12	13:06	30	0.82	Cloudfree	~~Canon~~ IXUS	135	0787 - 0921	Yes		
12	14/12	13:41	42	1.43	Cloudfree	~~Canon~~ IXUS	213	0922 - 1134	Yes		
13	14/12	14:28	15	0.41	Cloudfree	~~Canon~~ IXUS	65	1135 - 1199	Yes		
14	14/12	17:03	34	1.23	Cloudfree	~~Canon~~ IXUS	196	1200 - 1395	Yes		
15	15/12	12:45	29	1.31	Scattered/~~l~~low clouds	~~Canon~~ IXUS	198	1396 - 1593	No		
16	15/12	14:07	21	0.58	Scattered clouds*	~~Canon~~ IXUS	119	1594 - 1712	Yes		
17	15/12	14:30	30	1.16	Scattered clouds*	~~Canon~~ IXUS	196	1713 - 1908	Yes		
18	15/12	15:02	32	1.25	Scattered clouds*	~~Canon~~ IXUS	209	1909 - 2117	Yes		
19	15/12	15:49	15	0.16	Scattered clouds*	~~Canon~~ IXUS	37	2118 - 2154	Yes		
20	15/12	16:06	32	1.26	Scattered clouds*	~~Canon~~ IXUS	197	2155 - 2351	Yes		

* Illumination problems, probably due to light scattering associated to fog entering the caldera from the NE and the dark wall of the bordeira in the S and W, resulting in striping.

Take-off with the eBee is performed by hand, but landing needs several tens of meters of approach area, and a smooth landing surface in order not to damage the EPP UAV body. This was a significant limitation to the survey, since the area of the Chã das Caldeiras is mostly covered by very rough lava surfaces, with scarce smooth ash and lapilli cover sites. Given these constraints, five sites allowing for good landing conditions were selected (Fig. 3): i. 14.93477º N, 24.35407º W, ii. 14.928092º N, 24.353165º W, iii. 14.92339º N, 24.356605º W, iv. 14.9334999º N, 24.3722831º W and, v. 14.962204º N, 24.3690256º W.

~~The survey consisted of 20 flights that do not show the ideal spatial setup nor homogenous illumination conditions in the resulting aerial photos, but it was the best solution given the logistical constraints. This was due to the following problems: sparse location of the take-off and landing sites, changes in wind-speed affecting power consumption, unexpected cloud advection and low visibility during some days, duration of daylight, fast changing shadowing effect from the Bordeira rock wall and by Pico do Fogo, battery limitations (due to heat, high risk of damaging the UAV in case of a need to crash land over lava flows, we decided not to conduct flights of over 30 min) and, long-distances to move between landing sites, these resulting on the need for constant on-site modifications of the original flight planning. The average flight elevation above the ground was 190 m, resulting on an average ground sampling distance of 6 cm, over 2,900 aerial photos and a total surveyed area of 24 km^2 (Fig. 3).This setup was a compromise between the needs to map features of ci. 50 cm and the time available for the surveying, as well as battery limitations of the UAV.~~

Formatou: Inglês (Reino Unido)

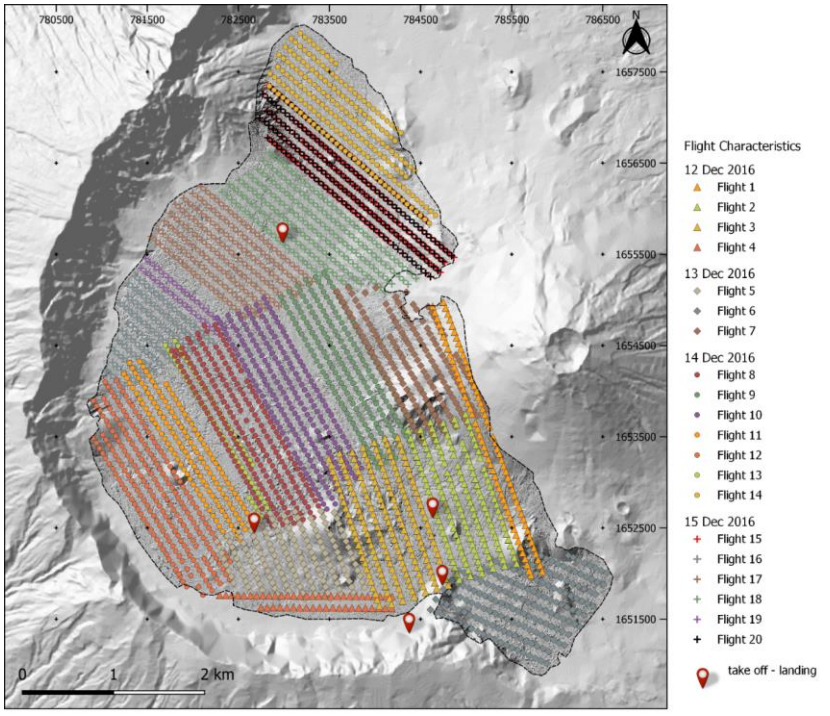

Figure 3 – General characteristics of the Aaerial survey of the Chã das Caldeiras with the geolocation of the photographs according to the flights, and take-off and landing locations ~~oosition of the two GNSS base stations, ground control points and accuracy checkpoints.~~, Shaded inside the survey area from the DSM produced here. Shaded relief outside the survey area ~~derived~~ from the DEMFI (2010) 5 m DEM.

The survey consisted of 20 flights with a design that results from ~~an~~the initial planning~~,~~ modified during the field work. The ~~results~~results do not show ~~an~~the ~~-~~ideal spatial setup nor homogenous illumination conditions ~~in the resulting aerial photos~~, but it was the best solution given the logistical constraints (Table 1). This was due to the following problems: sparse location of the take-off and landing sites, changes in wind-speed affecting power consumption, unexpected cloud advection and low visibility during some days, duration of daylight, fast changing shadowing effect from the Bordeira rock wall and Pico do Fogo, battery limitations (due to heat, high risk of damaging the UAV in case of a need to crash land over lava flows, we decided to avoid flights of over 35 min) and long-distances between landing sites. The survey consisted of over 2,900 aerial photos and on a total surveyed area of 24 km^2 (Fig. 3).

Formatada: Centrado

Formatada: Normal

43.2 Ground control points

Coordinates of ground control points (GCPs) were measured at markers distributed in the field prior to the survey and at easily identifiable points, such as large boulders and building edges. The measurements were obtained in December 2016 using a Leica Viva (GS08) dual frequency GNSS rover in RTK mode, with GNSS base stations located installed at known coordinate sites in high positions (Monte Beco and Monte Amarelo, Fig. 4) and at a maximum distance of 2.3 km from the between base and rover and a rover for surveying in RTK mode during the field surveys in December 20182016. The coordinates of the base stations were obtained using the base station FGMB00CPV (Fogo - Monte Beco) of the Instituto Nacional de Gestão do Território (INGT). The collection of each GCP was done once the positioning accuracy stabilized below 2 cm. Extra GCPs were collected in February 2017 in small boulders selected in the preliminary orthophoto mosaic, in orderwith the objective to of improvinge georeferencing quality. These points were obtained by post-processing using the FGMB00VCPV, since some were at high distance from the base. The accuracy of the GNSS positioning GCP coordinates is of about 3 cm plus the uncertainty in the precise positioning of the rover in relation to the terrain feature, which we estimate to be of about 5-10 cm. The GCP coordinates are provided in the dataset, with the coordinate system WGS 84 UTM Zone 26N.

4.3 Point cloud, orthophoto mosaic and digital surface model

Aerial image processing was done using Pix4Dmapper 4.5.6, a commercial software based on automatic feature detection, image matching and modelling using SfM algorithms. Extensive methodological reviews on the application UAV photogrammetry using this technique are found in Westoby et al. (2012), Smith et al. (2016) and Derring et al. (2019).

The point cloud was processed using the full image scale, matching of image pairs using the aerial grid/corridor model and geometrically verified matching using automatic advanced key points extraction. PIX4D does not disclose the exact algorithms used in the processing. The feature matching is based on the SIFT algorithm, with the PIX4D workflow being described in Küng et al (2011). The advanced camera calibration was done by: i. using the so-called alternative method, which is optimized for aerial nadir images with accurate geolocation, ii. optimizing all internal camera parameters, iii. Optimizing all external parameters (rotation and position) and, iv. no automatic rematch. The camera optimization resulted in a 0.35% difference between the initial and optimized internal camera parameters, with the point cloud having used 2909 out of the total 2919 images.

Formatada: Avanço: Primeira linha: 0 cm

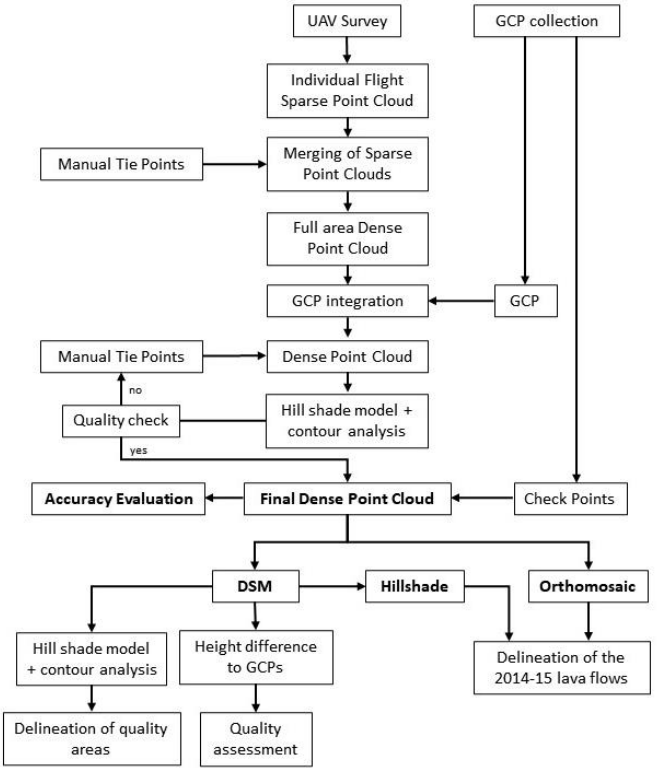

Figure 4 – Work flow from the field survey to the generation of the DSMs and orthomosaics.

Formatada: Centrado

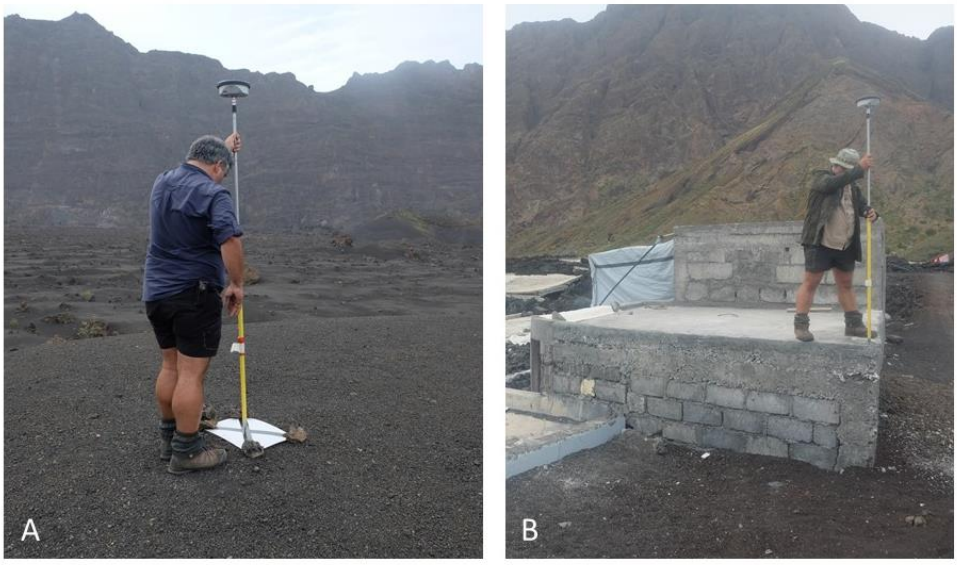

~~**Figure 4 – Ground control point collection with RTK GNSS. A. Using markers, B. Using existing points.**~~

515

~~3~~4.3 Point cloud, orthophoto mosaic and digital surface model

~~Aerial image processing was done using Pix4Dmapper 4.5.6, a commercial software based on automatic feature detection, image matching and modelling using structure from motion (SfM) algorithms. Westoby et al. 2012; Smith et al. 2016)This process developed in the 1990s, results from the application of algorithms by automatic feature matching. The~~ 520 ~~SfM operates according to the basic principles of stereoscopic photogrammetry, in which a 3D structure results from a series of 2D image overlays taken in motion to an object. The geometry of the images, position and orientation of the camera are calculated automatically without the need for a priori indication. Decisions are made simultaneously based on an iterative adjustment of package images, and the structures are automatically extracted from several overlapping images and the points are searched from image to image allowing the estimation of the coordinates of the objects. The 3D point clouds are~~ 525 ~~generated in an image space coordinate system and are transformed into an absolute real-world object space coordinate system. The transformation is achieved by using 3D functions based on a relatively small number of GCPs (Westoby et al. 2012; Smith et al. 2016).~~

~~the The camera optimization resulted in a 0.35% difference between the initial and optimized internal camera parameters, with the point cloud having used 2909 out of the total 2919 images. The images showed a median of 49521 key points per image and a median of 22632 matches per calibrated image.~~

~~The models that we have developed have used 2909 calibrated images with an average ground sampling distance of 7.17 cm and a total area covered of 23.89 km². The camera optimization resulted in a 0.35% difference between the initial and optimized internal camera parameters. The images showed a median of 49521 key points per image and a median of 22632 matches per calibrated image.~~ The point cloud densification was done using multiscale and half-image size, with ~~an~~ optimal point density and a minimum number of 3 matches. This option was selected after intensive testing with 4 and 5 matches, which generated large gaps in the point clouds in areas that were well-resolved with 3 matches. Filtering of the point cloud was attempted in CloudCompare for ~~solving~~ outlier issues in poorly resolved areas, but as outliers were removed in some areas, others which were originally well-resolved, deteriorated. Hence, the full processing was conducted within PIX4D. ~~The point cloud still shows sectors with no data in homogeneous fine ash and lapilli covers, but those areas, as discussed below, are small and always outside the recent lava fields (Fig. 5). Since the target of the 3D survey are the lava fields, we guarantee that those sectors are well represented with an accurate point cloud (see next section).~~

The large number of flights, large area and different illumination conditions led us to do separate processing and georeferencing of flights, with iterative project merging until the final model was obtained (Fig. 4). For this procedure, individual flights were always processed initially for the generation of the sparse point cloud. We have then merged the adjacent flights done in the same day and conducted a visual inspection of the point cloud ~~in~~ order to identify poorly projected points in the overlapping sectors between adjacent flights. ~~In order to~~To guarantee improved matching, manual tie points (MTP - small features visible in the images, normally allowing for x~~,~~ and y accuracy better than 10 cm) were added at this stage and the model was reoptimized. ~~A similar procedure was done in the following step, after merging the flights from different dates.~~ Once the merge of the total surveyed area was completed, a total of 37 3D (x, y and z coordinates) and 3 2D (x and y coordinates) GCPs measured in the terrain were inserted in the point cloud (Fig. 5) and the model was reprocessed (rematched). Following this initial stage, an initial 10 cm resolution DSM was produced.

From the initial ~~digital surface model~~DSM ~~that was generated~~, a hill shade model was created, as well as a contour lines with 50 cm elevation distance. These were ~~then~~ used for a new detailed visual inspection of artefacts generated by the interpolation ~~by~~due to gaps in the point cloud or ~~by the interpolation of~~by outliers (Fig. 4). The main issues occurred in areas between adjacent flights or in sectors of very homogeneous terrain. In those sectors, more ~~manual tie points~~MTPs were added, until the artefacts disappeared. The procedure was done iteratively until no artefacts were found, except those associated to the lack of matches in the point cloud, mainly associated to homogeneous surfaces covered by pyroclasts (lapilli and ash). This detailed visual inspection of the hill shade model and contours also ~~approach also~~ solved issues related to different illumination conditions. Extra MTPs were further marked regularly over the point cloud to guarantee improved quality. To speed up the processing, when correcting specific sectors of the model, small processing areas were used. ~~The~~

Formatada: Justificado, Espaçamento entre linhas: 1,5

Formatada: Esquerda, Espaçamento entre linhas: simples

Formatou: Não Realce

Formatou: Não Realce

Formatou: Não Realce

Formatou: Não Realce

Formatou: Não Realce

~~procedure was done iteratively until no artefacts were found, except those associated to the lack of matches in the point cloud, mainly associated to homogeneous surfaces covered by pyroclasts (lapilli and ash).~~ ~~In this process, we have used a total of 37 3D and 3 2D GCPs measured in the terrain. In order to improve the matching,~~The full procedure ~~was very long~~ ~~and~~ involved the identification of 696 manual tie points ~~for~~ for the whole model (Fig. 5). Each tie point was ~~manually~~ identified in at least 3 images, but usually in more, with an average number of 10 images used. The insertion of a tie point was complete when the terrain feature used for identifying ~~the tie~~the point and its modelled projection in non-marked images were overlapping. The average projection error of the MTPs was 0.99 pixels, with a standard deviation of 0.6 pixels.

The detailed report of the PIX4D project is available in the data set and provides a detailed overview of the processing characteristics (cha_caldeiras_pix4d_report.pdf).

~~**were included, especially in areas covered by pyroclasts (lapilli and ash).**~~

Formatada: Legenda

~~The point cloud was processed using full image scale, matching of image pairs using the aerial grid/corridor model and geometrically verified matching using automatic advanced key points extraction. The advanced camera calibration was done using the alternative method, internal parameters optimization (all), external parameters optimization (all) and no automatic rematch. The point cloud densification was done using multiscale and half-image size, with an optimal point density and a minimum number of 3 matches. This option was selected after intensive testing with 4 and 5 matches, which generated large gaps in the point clouds, in areas which were well resolved with 3 matches. The point cloud still shows sectors with no data in homogeneous fine ash and lapilli covers, but those areas are small as discussed below and always outside the recent lava fields (Fig. 5). Since the target of the 3D survey are the lava fields, we guarantee that those sectors are well represented with many accurate points in the cloud.~~

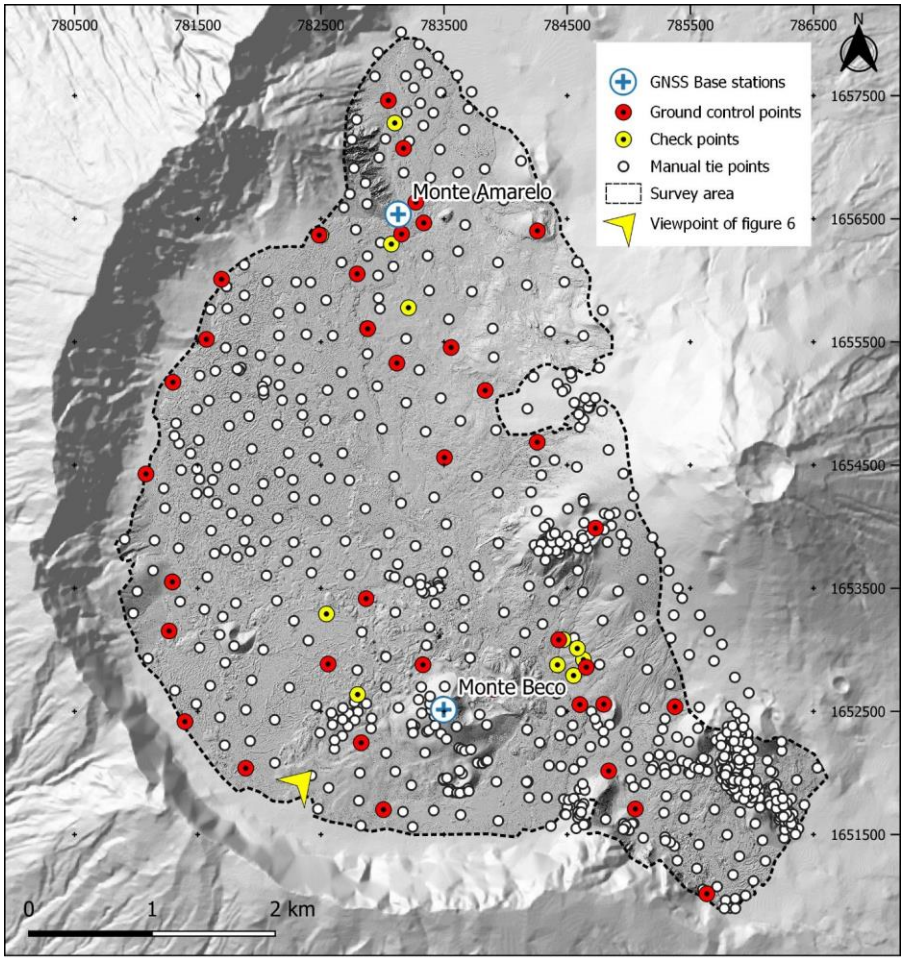

Formatada: Centrado

Figure 5 – Ground control points used for the model and for the accuracy evaluation (check points), manual tie points used to improve the point cloud accuracy and location of the GNSS base stations set up for collecting the ground control points and tie points. Shaded relief outside the survey area from the DEMFI (2010) 5 m DEM.

Formatada: Legenda

590

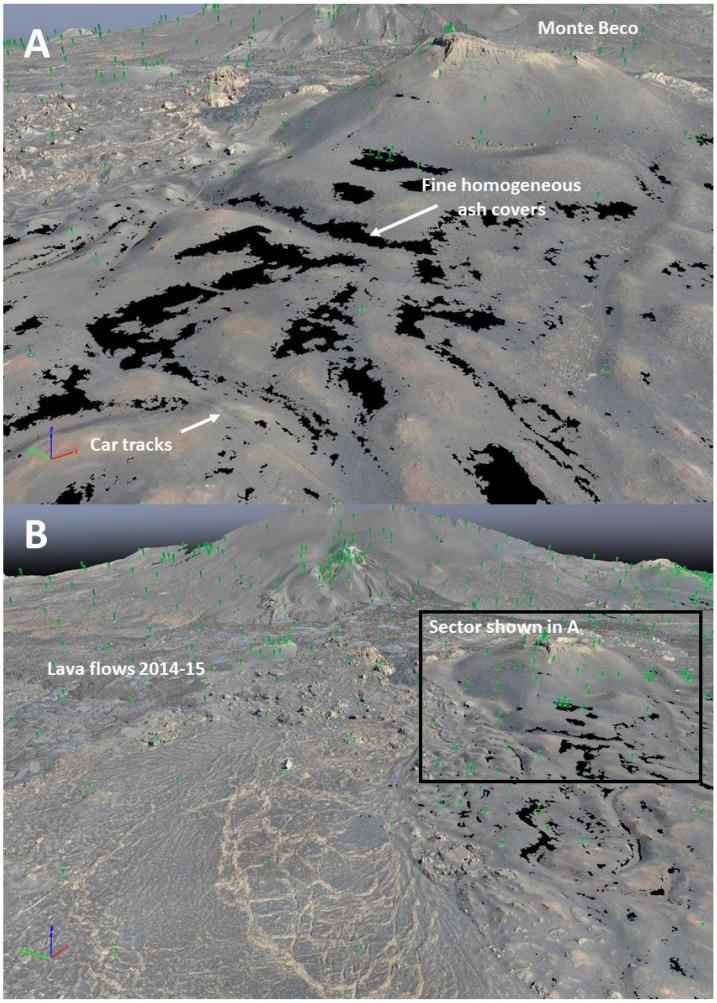

~~Figure 5 – Examples of areas without data in the 3D dense point cloud. A. Low quality areas in ash surfaces close to Monte Beco (car tracks pointed for scale), B. Most of the survey is of very high quality, with the figure showing the lava fields close to Monte Beco and the small areas with low quality. The green pins are manual tie points.~~

~~Despite producing a DSM and an orthomosaic with a 10 cm/pixel resolution that are also available in the dataset, T~~the ~~final main products are a~~ digital surface model (DSM) and orthomosaic ~~are presented with a resolution of 25 cm/pixel, which allowing for maintaining the root mean square error (RMSE) well below pixel size.~~ The DSMs with 10 and 25 cm/pixel were ~~was~~ interpolated in PIX4D using ~~the N~~noise filtering and sharp surface smoothing options in PIX4D ~~were applied for the DSM~~, with interpolation using inverse distance weighting. This set of options allows to remove erroneous points from the cloud by using the median elevation of neighbouring points, and ~~–~~smooths small bumps in the model, preserving sharp features, with only quasi-planar surfaces being flattened~~the sharp details of the a'a' lava field surfaces, but filters potential outliers in the point cloud in areas where point density is small~~. After comparing the different filtering options, this was the one that produced the best~~tter~~ results. The orthomosaics were produced with the same resolutions of the DSM in PIX4.

~~4~~3.4 Delineation of the low accuracy areas in the orthomosaic and DSM

Despite the ~~correction procedures,~~workflow with integration of numerous MTPs, the final densified point cloud ~~still~~ shows small sectors with no data in homogeneous fine ash and lapilli covers (Fig. 6). These ~~are~~respect to surfaces outside the main aim of this work, which ~~are~~is the mapping of the recent lava flows ~~that are accurately represented~~. However, since the UAV survey covers an area much larger than the lava flows of 2014-15 and most of it shows a very dense point cloud, and given their potential application for land management and research, we decided to make available the full survey results~~, due its potential impacts for land management and research~~. To provide the user with a quality zonation of the DSM~~As such~~, other than the evaluation of height error at GCPs, we ~~defined~~have followed a ~~subjective~~qualitative methodology for the delineation of three quality areas ~~of the areas with different point cloud quality, which allows the user to identify the limitations of the different surveyed areas~~.

~~Hence, the surveyed area was divided in three quality zones. For the assessment,~~The assessment was based in the analysis of the 10 cm/pixel shaded relief model~~, as well as~~ and the 50 cm equidistance contours. These were subject ~~interpolated from the DSM were used for~~ to a ~~a~~ systematic visual ~~analysis~~inspection that allowed for the ~~and for~~ manual delineation of the areas with errors in the DSM, in a procedure similar to the one used to add MTPs described in 4.3. This approach does not aim at calculating the accuracy of the DSM, but rather at identifying the areas that should not be used for quantitative purposes.

The following criteria were used ~~to define the zones~~:

- The ~~H~~high-quality areas~~:~~ are those where the point cloud is dense and has no relevant gaps, resulting in good interpolation with the hill shade model and contours showing regular features, describing accurately the terrain surface. These areas ~~coincide with areas of~~correspond generally to rough surfaces with numerous automatic and manual tie points, where the morphology is ~~very~~ accurate, and the point cloud ~~model~~ has high-resolution (Figures 6 and 7). ~~;~~
- Medium-quality: sectors dominated by ash and lapilli, where sporadic 3D errors occur (Fig. 7-A and B). These areas can be used for visualization purposes and even for quantification, but with special care. Most errors in these

Formatou: Não Realce
Formatou: Não Realce
Formatou: Não Realce
Formatou: Não Realce
Formatou: Não Realce
Formatou: Não Realce
Formatou: Não Realce
Formatou: Não Realce
Formatou: Não Realce
Formatou: Não Realce
Formatou: Não Realce
Formatada: Avanço: Primeira linha: 1,27 cm
Formatou: Não Realce

zones are very small (dm scale) and can be smoothed by resampling, for example to 1-2 m resolution. The errors are visible by small artefacts in the hill shade model and in the contour lines.

- Low-quality: patches where the point cloud was poorly resolved, having numerous artefacts in the DSM as seen in the hill shade model and also in the contour lines (Fig. 7-C and D). These areas cannot be used for quantification purposes and their visualization shows errors, which sometimes are significant.

Formatada: Parágrafo da Lista, Com marcas + Nível: 1 + Alinhado a: 0,63 cm + Avanço: 1,27 cm

Formatou: Não Realce

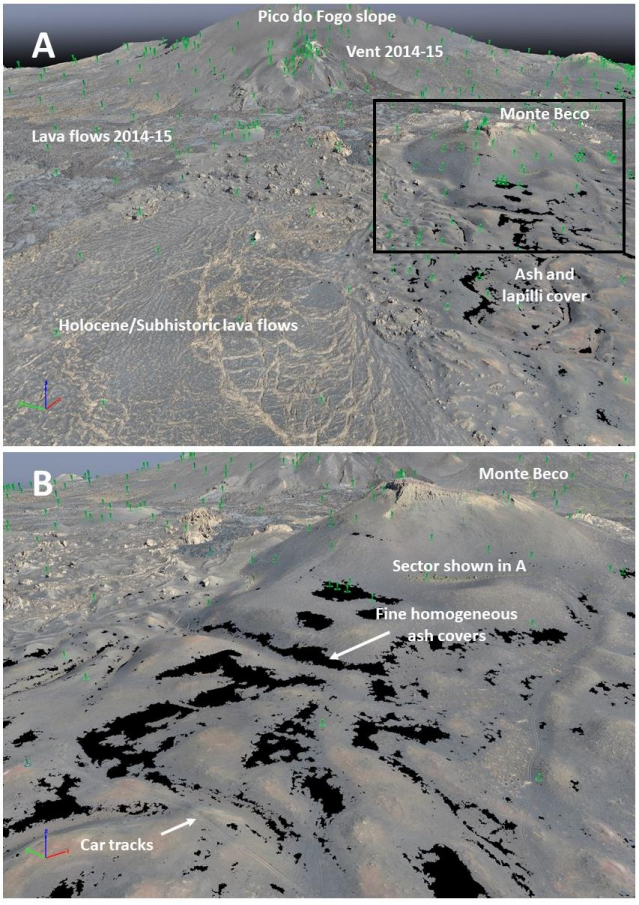

Figure 6 – Examples of the quality of the 3D dense point cloud. A. Most of the point cloud shows dense point coverage and high accuracy, with the figure showing the lava fields close to Monte Beco and the small areas with gaps and low quality. B. Low quality areas in ash surfaces close to Monte Beco (car tracks for scale), The green pins are manual tie points. The location of the sector covered in this figure is indicated in Fig. 5.

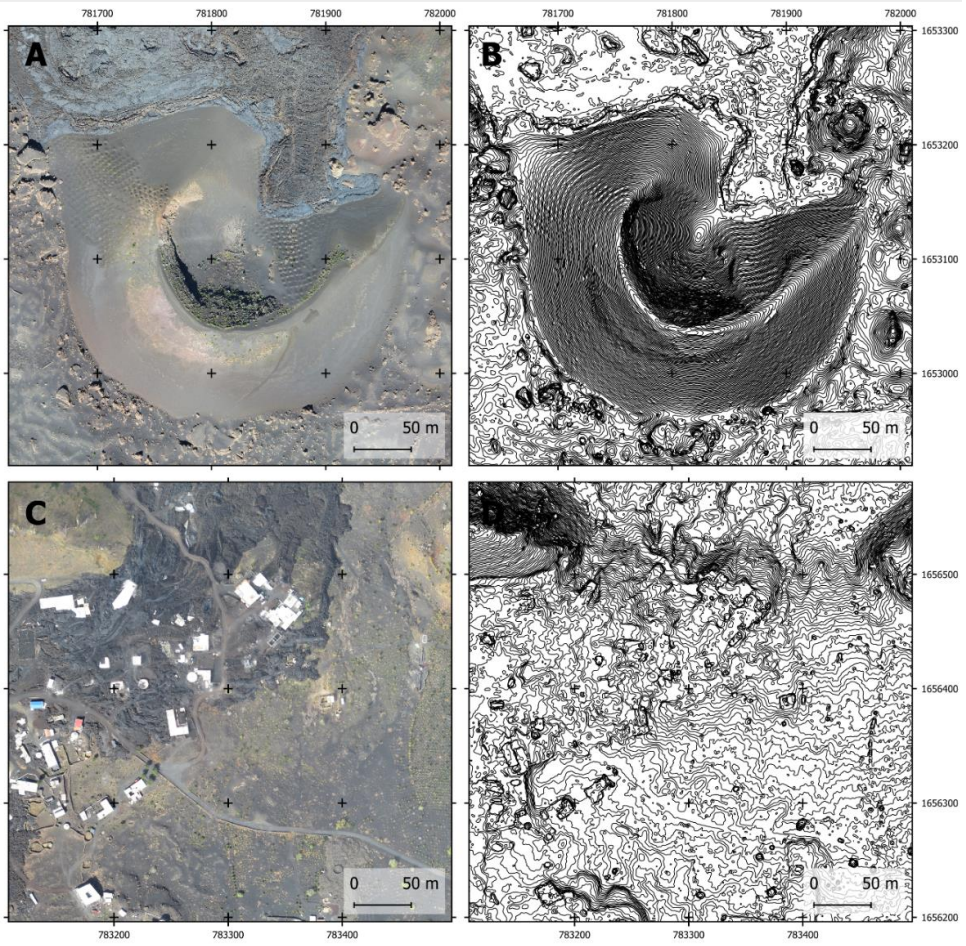

Figure 119 – Examples of surfaces in the Chã das Caldeiras with high-quality results for the digital surface model, with orthomosaic for visualization (10 cm resolution) and contour lines derived from the digital surface model (50 cm equidistance). Note the good quality of the elevation contours. A and B. Volcanic cone with cultivated areas inside the crater, C and D. Lava field with buildings and a road.

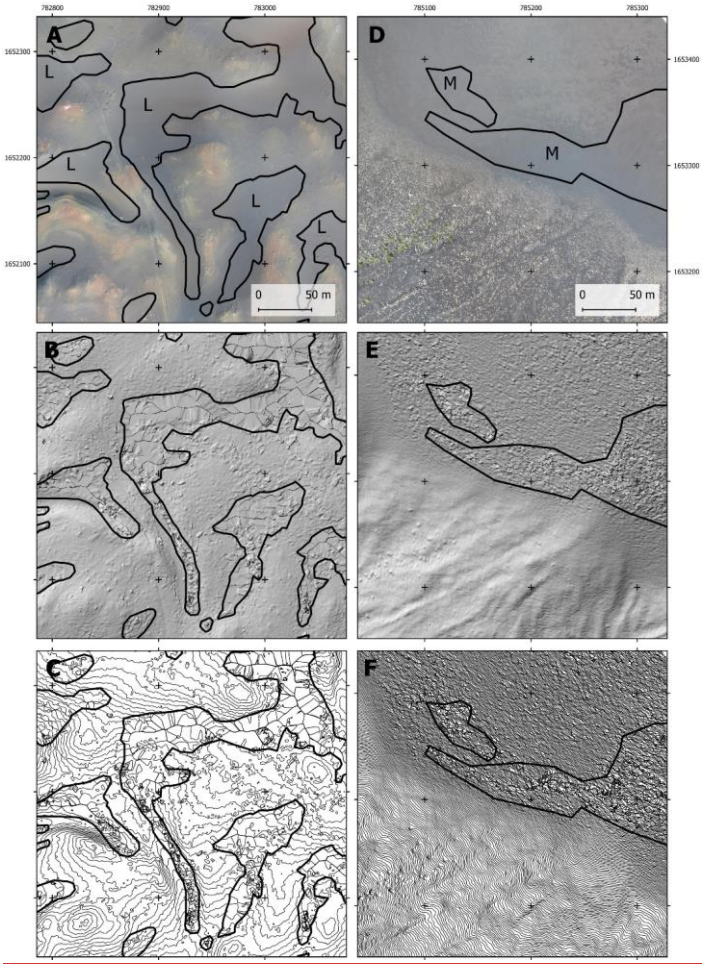

650

~~Medium-quality: sectors dominated by ash and lapilli, where sporadic 3D errors occur. These areas can be used for visualization purposes and even for quantification, but with special care. Most errors in these zones are very small (dm scale) and can be smoothed by resampling, for example to 1-2 m resolution.~~

Formatada: Centrado

Formatada: Normal, Sem marcas nem numeração

~~Low-quality: patches where the point cloud was poorly resolved, having numerous artefacts in the DSM. These areas cannot be used for quantification purposes and their visualization shows errors, which sometimes are significant.~~Figure 7 – Examples of surfaces with high, medium and low quality in the DSM. A-C: Steep slope covered with ash with medium-quality results (M) for the digital surface model (A - orthomosaic, 10 cm, B – Hill shade model, 10 cm, C - contour lines, 50 cm). The contours are very irregular in detail, but the overall slope at a coarse resolution is maintained. The area where the deposits are coarser (outside the polygon) provides a good DSM. D-F: Irregular surfaces with linear depressions covered with ash with low-quality results (L), with orthomosaic for visualization (A - orthomosaic, 10 cm, B – Hill shade model, 10 cm, C - contour lines, 50 cm). The contours are very irregular and show numerous errors. The border with the good quality areas is sharp with good topography where the ground surface is coarser. The location of the figures is shown in Figure 12.

Formatada: Legenda

Formatada: Normal, Sem marcas nem numeração

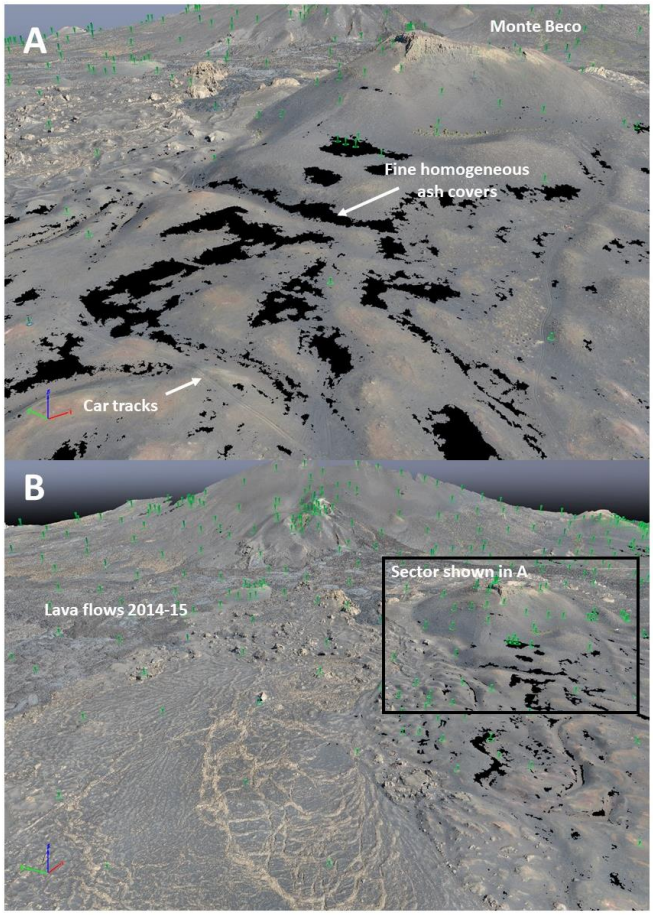

Figure 6 – Examples of the quality of the 3D dense point cloud. A. Low quality areas in ash surfaces close to Monte Beco (car tracks for scale), B. Most of the point cloud shows dense point coverage and high accuracy, with the figure showing the lava fields close to Monte Beco and the small areas with gaps and low quality. The green pins are manual tie points. The location of the sector covered in this figure is indicated in Fig. 5.

Formatada: Título 2

Formatada: Título 2, Esquerda

Formatada: Título 2

~~n order to guarantee the quality of its use,applications, the DSM was divided in three quality zones (Fig. 7). The zonation is available in the dataset as a shapefile that can be used to mask the DSM depending on user needs. The high resolution (10 cm) shaded relief model derived from the DSM, as well as the 50 cm equidistance contours interpolated from the DSM were used for the systematic visual analysis and for manual delineation of the areas with errors in the DSM. The following criteria were used to define the zones:~~

~~High-quality: coincide with areas of rough surfaces with numerous automatic and manual tie points, where the morphology is very accurate, and the point cloud model has high resolution;~~

~~Medium-quality: sectors dominated by ash and lapilli, where sporadic 3D errors occur. These areas can be used for visualization purposes and even for quantification, but with special care. Most errors in these zones are very small (dm scale) and can be smoothed by resampling, for example to 1-2 m resolution.~~

~~Low-quality: The low-quality zones correspond to patches where the point cloud was poorly resolved, having numerous artefacts in the DSM (Fig. 11). These areas cannot be used for quantification purposes and their visualization shows errors, which sometimes are significant.~~

~~The zonation is available in the dataset as a shapefile that can be used to mask the DSM depending on user needs.~~

43.5 Delineation of the 2014-15 lava ~~-~~flow field

The lava flow field of the 2014-15 eruption (Fig. 1) was digitized manually using the orthomosaic ~~and DSM~~, hill shade model and contour lines ~~(Fig. 1)~~ and is made available in the data set. Our knowledge of the field conditions and the high-resolution of the orthomosaic allowed for the accurate delineation of the contact between the lava flows and the adjacent surfaces, which is sharp and well-defined. We have delineated both the external limit~~s~~ of the flows, as well as the internal, when it surrounded landforms such as kīpukas. The delineation covered the full-data set, but unfortunately ~~Our~~the UAV survey missed a small area of the lava flow with 0.007 km^2 in the northwest sector of Chã das Caldeiras, close to Monte Amarelo ~~and~~. Therefore, that sector has been ~~to be~~ digitised using very high-resolution Google Earth imagery. The delineation procedure was done in QGIS by manual vectorization and an example is shown in figure 7.

Formatada: Título 2, Sem marcas nem numeração

Formatada: Título 2

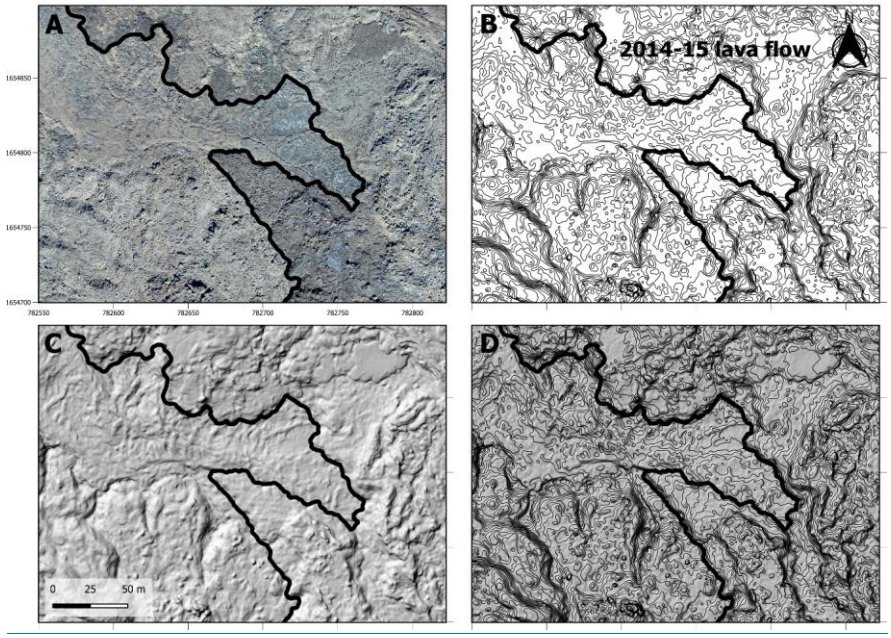

Figure 8 – Example of manual delineation of the lava flow by making use of the: A. Orthomosaic, B. Elevation contours with 50 cm interval, C. Hill shade model, D. Hill shade model and elevation contours.

5. Results and discussion

5.1 Point cloud and DSM

The densified point cloud covers a total area of 23.89 km^2 with an average ground sampling distance of 7.17 cm, with and a median of 22632 matches per calibrated image. The full point cloud has an average of 15.9 points/m^2 and a standard deviation of 6.5 points/m^2 (Table 2), with most of the area showing values above 15 points/m^2 (Fig. 10). The least accurate areas, with less than 5 points/m^2 are spatially limited and locate mainly close to the limits of the survey, where there was less aerial coverage. Some small sectors west of Monte Beco and of Monte Orlando also show low density, but those are associated to very regular surfaces of ash and lapilli (see Fig. 7). The sector between Portela and Bangaeira shows a narrow

Formatada: Centrado

Formatada: Legenda

Formatou: Superior à linha

Formatou: Superior à linha

Formatou: Superior à linha

NW-SE corridor with a width of around 90 m and a length of about 1200 m with 6-8 points/m^2, caused by hazy conditions that reduced scene contrast. However, the topography is relatively regular and hence the point cloud quality is good , lacking artefacts. The area of the 2014-15 lava flows show a better overall quality of the point cloud, with a mean of 18.3 points/m^2 (Table 2). This value is clearly affected by the average quality of the Portela-Bangaeira area, with most of the lava flows showing much higher densities (Fig. 9), as revealed by the bimodal histogram of figure 10.

Table 2 – Point density in selected areas of the Chã das Caldeiras point cloud

	Mean (points/m^2)	Median (points/m^2)	Standard Deviation (points/m^2)
Full Point Cloud model	15.9	15.9	6.5
DSM Area	16.8	16.5	5.9
Lava flows 2014-15	18.3	17.7	6.9

Formatou: Superior à linha

Formatou: Superior à linha

Formatada: Legenda, Centrado

Formatou: Tipo de letra: 10 pt, Inglês (Reino Unido)

Tabela Formatada

Formatou: Tipo de letra: 10 pt

Formatou: Tipo de letra: 10 pt

Formatou: Tipo de letra: 10 pt

Formatou: Tipo de letra: 10 pt

Formatou: Tipo de letra: 10 pt

Formatou: Tipo de letra: 10 pt

Formatou: Tipo de letra: 10 pt

Formatou: Tipo de letra: 10 pt

Formatou: Tipo de letra: 10 pt

Formatou: Tipo de letra: 10 pt

Formatou: Tipo de letra: 10 pt

Formatou: Tipo de letra: 10 pt

Formatou: Tipo de letra: 10 pt

Formatou: Tipo de letra: 10 pt

Formatada: Legenda, Centrado

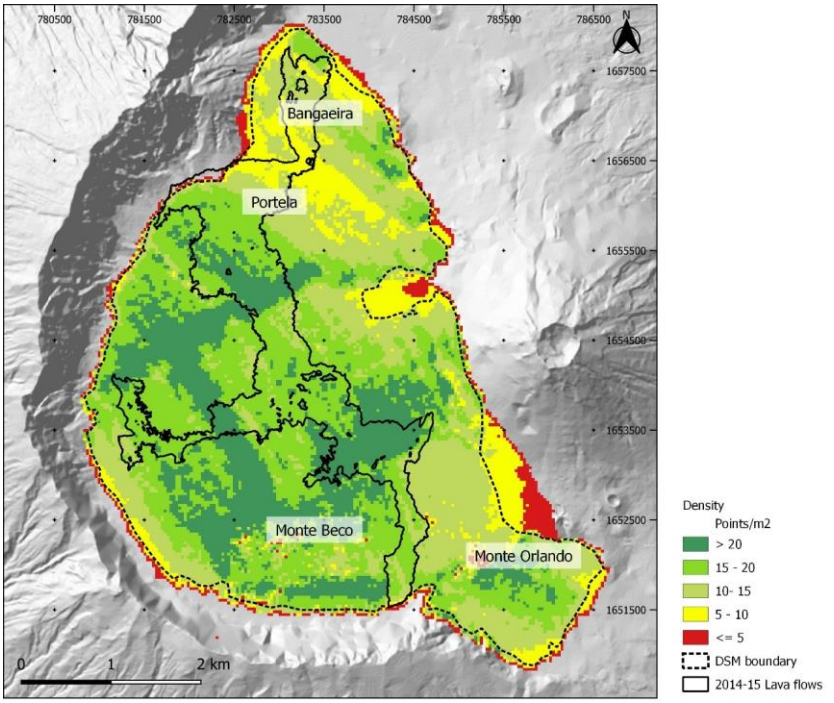

Figure 9 – Density of the point cloud of Chã das Caldeiras.

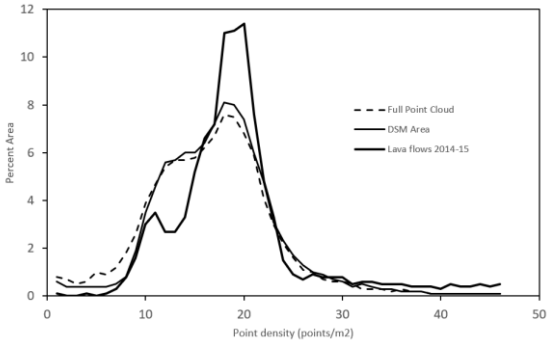

725

Formatada: Centrado

Figure 10 – Point density frequencies in selected areas of the Chã das Caldeiras point cloud.

The georeferencing accuracy of the point cloud was ~~verified~~assessed using 13 independent check points~~, which have been~~ measured with dGPS in the field ~~and~~ that were not used for the modelling~~.~~. The point cloud ~~and model shows a~~ RMSE ~~of~~ is 0.08 m in X, 0.11 m in Y and 0.12 m in Z, with the projection error being always below 1.03 pixels~~, evaluated using 13 independent check points~~ (Table 3~~2~~1). This is over one order of magnitude better than the 1 m DEM by Bagnardi et al. (2016).

~~Even a~~After ~~including~~ adding ~~several hundreds of manual tie points, it was not possible to obtain a~~ very good quality point cloud ~~in most of the surveyed~~ all over the survey area. ~~However, A~~areas of homogeneous ash and pyroclasts covers lack 3D ~~data, but they do not impact the overall mapping of the area, as is discussed below.~~

Table 3~~2~~1 – Accuracy of the densified point cloud ~~Location accuracy~~ per ~~Ground Control~~check ~~P~~point in X, Y and Z.

Check Point ID	Error X (m)	Error Y (m)	Error Z (m)	Projection Error (pixels)
beco03	-0.0218	-0.0110	0.0729	1.02
beco05	-0.1511	-0.1224	-0.0617	0.40
beco10	-0.0597	0.0347	0.2638	0.45
beco23	-0.0026	0.0791	0.0287	0.39
beco24	-0.0076	0.0844	0.1193	0.53
beco26	0.0286	0.1193	-0.0298	0.52
beco28	0.0671	0.0423	-0.0542	0.28
beco29	-0.0872	-0.0194	-0.1591	0.54
amarelo03	-0.0451	-0.1036	0.0280	0.41
amarelo05	-0.1162	-0.3011	0.2447	0.80
amarelo13	0.0567	0.0098	-0.1135	0.97
amarelo14	0.1900	0.0138	0.1076	0.74
amarelo16	-0.0011	0.1119	0.0940	0.60
Mean (m)	-0.0107	-0.0045	0.039	
RMSE (m)	0.082	0.107	0.125	

5.2 Digital Surface Model

The point cloud interpolation allowed generating DSM and orthomosaics with 10 and 25 cm/pixel resolution. In this manuscript we use the former for visualization purposes, but we recommend, for quantitative analysis, to use the digital surface model and orthomosaic with 25 cm/pixel. This will allow to keep the root mean square error (RMSE) of the point cloud well below pixel size (table 3). The DSMs show very high topographic detail and allow for excellent visualization and

Formatada: Centrado
Tabela Formatada
Formatada: Centrado
Formatada: Centrado
Formatada: Centrado
Formatada: Centrado
Formatada: Centrado
Formatada: Centrado
Formatada: Centrado
Formatada: Centrado
Formatada: Centrado
Formatada: Centrado
Formatada: Centrado
Formatada: Centrado
Formatada: Centrado
Formatada: Centrado
Formatada: Centrado
Formatada: Centrado
Formatada: Centrado
Formatada: Título 1

quantification of the terrain morphometry (Fig. 11). In order to avoid the use of the areas where the point cloud shows lower point density, the DSM were clipped and are smaller than the original point cloud, showing a mean point density statistics of 16.8 points/m^2 (Table 2 and Figures 10 and 11).

Formatou: Superior à linha

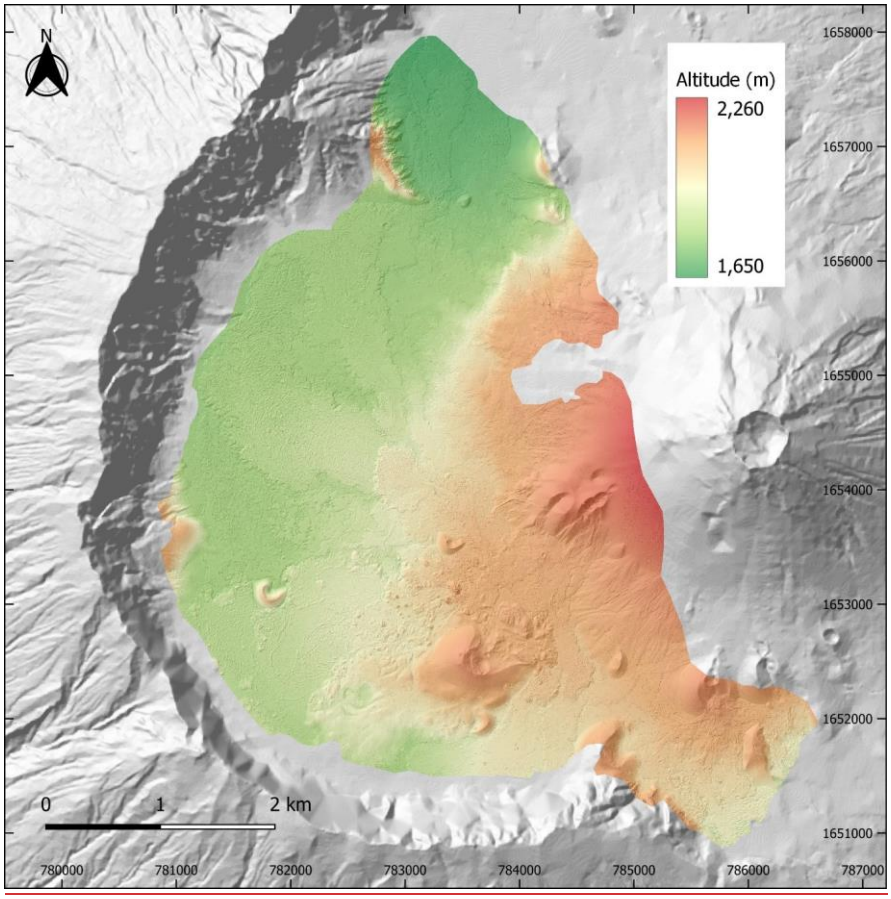

Figure 11 – Digital surface model of the Chã das Caldeiras with a transparency of the DSM shaded relief model. The surveyed area is overlaying the DEMFI (2010) 5 m DEM.

For evaluating the elevation accuracy of the DSM, elevations were compared with the ground control points obtained with differential GNSS. The results show a mean height difference of -0.13 m, a RMSE of 0.4 m and a standard deviation of 0.38 m (Table 4). Figure 12 shows the spatial distribution of the differences to the GCPs with three outliers with larger errors

Table 4 – Altitude differences between the digital surface model of the Chã das Caldeiras (25 cm/pixel) and the ground control points measured with differential GNSS in the field.

GCP-ID	Altitude GCP (m)	Altitude DSM (m)	Height difference (m)	Height difference (no outliers) (m)
14-modified	1765.69	1765.75	0.06	0.06
18modified	1908.23	1908.63	0.39	0.39
amarelo02	1683.50	1683.54	0.03	0.03
amarelo03	1692.52	1692.66	0.14	0.14
amarelo04	1702.10	1701.92	-0.19	-0.19
amarelo06	1719.79	1720.07	0.28	0.28
amarelo07	1739.94	1739.39	-0.55	-0.55
amarelo08	1756.43	1756.28	-0.15	-0.15
amarelo10	1769.58	1769.70	0.12	0.12
amarelo11	1769.63	1769.53	-0.11	-0.11
amarelo12	1776.71	1776.69	-0.02	-0.02
amarelo13	**1772.26**	**1770.86**	**-1.41**	-
amarelo14	1760.51	1760.08	-0.42	-0.42
amarelo15	1770.25	1770.05	-0.20	-0.20
amarelo16	1769.81	1769.53	-0.28	-0.28
beco01	1846.95	1846.89	-0.07	-0.07
beco02	1812.86	1812.89	0.03	0.03
beco03	1802.32	1801.68	-0.64	-0.64
beco04	1787.39	1787.43	0.04	0.04
beco05	1805.41	1805.56	0.15	0.15
beco06	1799.27	1799.28	0.01	0.01
beco07	1808.14	1808.10	-0.04	-0.04
beco09	1773.58	1773.39	-0.19	-0.19
beco10	1776.18	1775.64	-0.54	-0.54
beco10	1776.18	1775.64	-0.54	-0.54
beco11	1786.35	1785.84	-0.51	-0.51
beco13	1778.42	1778.29	-0.12	-0.12
beco17	1826.10	1825.96	-0.14	-0.14
beco18	1844.23	1843.71	-0.52	-0.52
beco22	1856.90	1856.98	0.08	0.08
beco23	1851.84	1851.93	0.09	0.09
beco24	1853.84	1853.93	0.09	0.09
beco26	1844.78	1844.85	0.08	0.08
beco27	1850.15	1850.26	0.11	0.11
beco28	1839.60	1839.70	0.10	0.10
beco29	1838.35	1838.59	0.24	0.24
beco30	1826.60	1826.88	0.28	0.28
GCP1	1814.15	1814.18	0.03	0.03
GCP2	1797.38	1797.23	-0.15	-0.15
GCP20	1782.71	1782.65	-0.06	-0.06
GCP3	1869.63	1869.82	0.20	0.20
GCP6	2078.02	2078.55	0.53	0.53

Tabela Formatada

GCP7	**1812.78**	**1811.83**	**-0.95**	-
GCP8	1829.99	1829.85	-0.14	-0.14
GCP9	1797.09	1797.14	0.05	0.05
GCP11	**1810.80**	**1809.62**	**-1.19**	-
GCP15	1759.49	1759.52	0.03	0.03
Mean			-0.13	-0.06
RMSE			0.40	0.27
STD			0.38	0.26

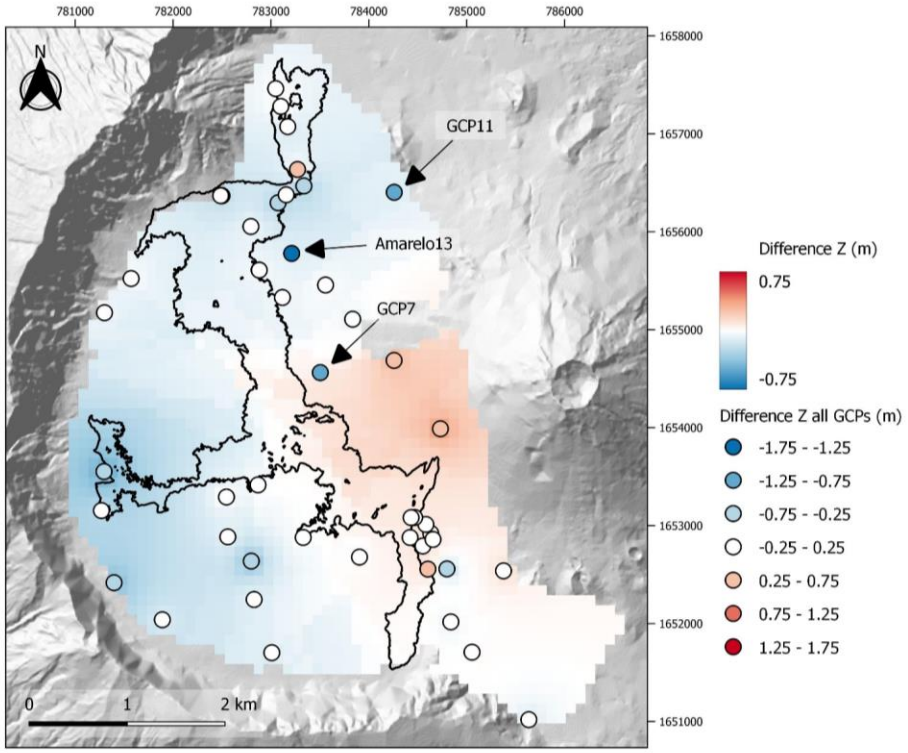

Figure 12 – Height differences between ground control points and the digital surface model of the Chã das Caldeiras (25m/pixel). The interpolated surface does not consider the 3 outliers which were measured on the top edge of built vertical surfaces.

Formatada: Legenda

Formatada: Justificado, Espaçamento entre linhas: 1,5 linhas

indicated with arrows (Amarelo13, GCP7 and GCP11). Amarelo13 and GCP7 were measured at corners in the top of walls, while GCP11 is the top of a large concrete geodetical benchmark. All these points that were accurately marked in the point cloud, lay above the topographic surface, which shows a significantly lower value after the interpolation of the DSM. Hence, these GCPs may be removed from the error assessment, since they will result in excess errors. Without the outliers, the mean height difference is -0.06 m, the RMSE is 0.27 m and the standard deviation is 0.26 m (Table 4).The interpolated raster and contours in figure 12 show the error surfaces not accounting for the three outliers, revealing the spatial distribution of the error in elevation. Positive errors (DSM higher than the GCPs) occur mainly in the western slope of Pico do Fogo, an area with steep slopes (>15º) and smooth surfaces. Negative errors show mainly in the western part of the area, closer to the Bordeira wall. The 2014-15 lava flows occupy an area with a mean estimated difference of -0.01 m and a standard deviation of 0.06 m, obtained from the interpolated surface from the GCP difference values. These values should be taken with care, since there is a small number of GCPs inside the lava flows, with the only ones having been obtained in the north of the Chã das Caldeiras.

~~As mentioned above, some areas of the point cloud and resulting DSM show lower quality due to the lack of point matches associated to very homogenous surface covers.~~ The qualitative assessment by visual inspection of the hill shade model and contours derived from the digital surface model, allowed for identifying ~~of the spatial distribution and representativity of these areas~~ different quality areas:~~The~~~~shows that the~~ high-quality zones cover 96.8% of the entire survey (Fig. 13). These ~~and~~ coincide with the areas of rough surfaces with numerous automatic~~-~~ tie points~~and manual tie points, where~~with the morphology reconstruction being~~is~~ very accurate, and the point cloud model ~~has~~showing high ~~resolution~~density ~~(Fig. 87).~~

The medium-quality zones are sectors dominated by ash and lapilli, where sporadic 3D errors occur and occupy 0.66% of the survey. The low-quality zones only occupy 2.64% of the survey area. These situations occur in very smooth surfaces of ash and lapilli or in sectors where a small number of overlapping aerial photos exists and where aerial photo resolution is not enough to resolve small features in the terrain. These areas are located mainly in the base of slopes, concave areas and also at the top of Monte Beco, due to problems photo coverage.

The 2014-15 lava flows do not show artefacts, except in a very small area of 600 m^2 located mid-way between Portela and Ilhéu de Losna, pointed in Figure 13 (A). This minor problem was due to the lack of overlap among aerial photos, which limited the point cloud generation. Within the recent lava flows, the ‘a'ā lava flow fields are characterized by high rugosity and numerous features which are easily matched between aerial photographs, including blocks, frequent sharp slope changes and pressure ridges. The Pāhoehoe lava flows show a much smoother and homogeneous surface, but they have frequent fractures and lineaments. They occupy generally small sectors of the orthomosaic and are bound by very rough a'ā lavas, facilitating point matching.

Formatada: Justificado, Espaçamento entre linhas: 1,5

Formatou: Inglês (Estados Unidos)

Formatou: Superior à linha

Formatou: Inglês (Estados Unidos)

4.2 Digital Surface Model

The DSM of the Chã das Caldeiras with 25 cm resolution shows unprecedented topographic detail and allows for excellent visualization and quantification of the terrain morphometry. The iterative improvement of the point cloud by a detailed visual analysis of the DSM shaded relief model followed by adding almost 700 manual tie points in the model and reprocessing, allowed to reach a very high-quality result (Fig. 6). The final model is the result of a resampling of the first model obtained with 10 cm resolution.

Formatada: Normal

In order to guarantee the quality of its use, the DSM was divided in three quality zones (Fig. 7). The zonation is available in the dataset as a shapefile that can be used to mask the DSM depending on user needs. The high-resolution (10 cm) shaded relief model derived from the DSM, as well as the 50 cm equidistance contours interpolated from the DSM were used for the systematic visual analysis and for manual delineation of the areas with errors in the DSM.

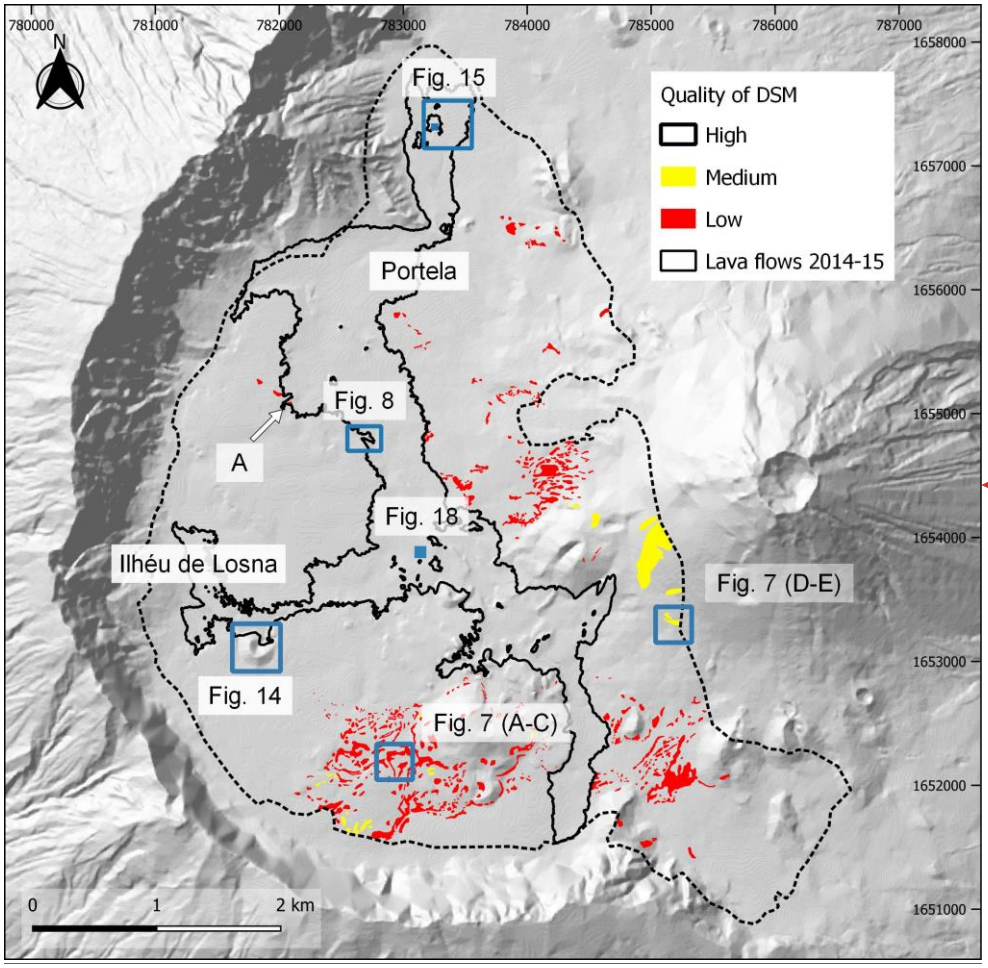

815

Formatada: Centrado

Figure 13~~8~~7 – Qualitative a~~A~~ssessment of the Qquality of the ~~dense point cloud and~~ digital surface model in the Chã das Caldeiras and location of the sectors shown in ~~figures 8 to 10~~different figures. The letter A indicates a small sector of the recent lava flow with low quality. Shaded relief outside the surveyed area derived from the DEMFI (2010) 5 m DEM.

~~The final DSM of the Chã das Caldeiras is presented here with 25 cm resolution. It shows very high topographic detail and allows for excellent visualization and quantification of the terrain morphometry (Fig. 9). This model is a lower resolution product derived from the point cloud from which we have also generated the 10 cm resolution DSM, which should be used with care due to the similarity of pixel size to the RMSE (8-12 cm, Table 2).~~

Figure 14 shows an examples of the resolution and quality of the DSM and orthomosaic. Areas with rough surfaces such as the small volcanic cones represented, show very high-quality results. The area shows a volcanic cone, a pahoehe lava flow in the NW sector and an ‘a'ā lava flow in the central part (Fig. 13 A and B). The magnified sector in C and D shows a large boulder and a gentle slope with small holes dug to cultivate vines, as well as other small trees, which are very well represented in the DSM.

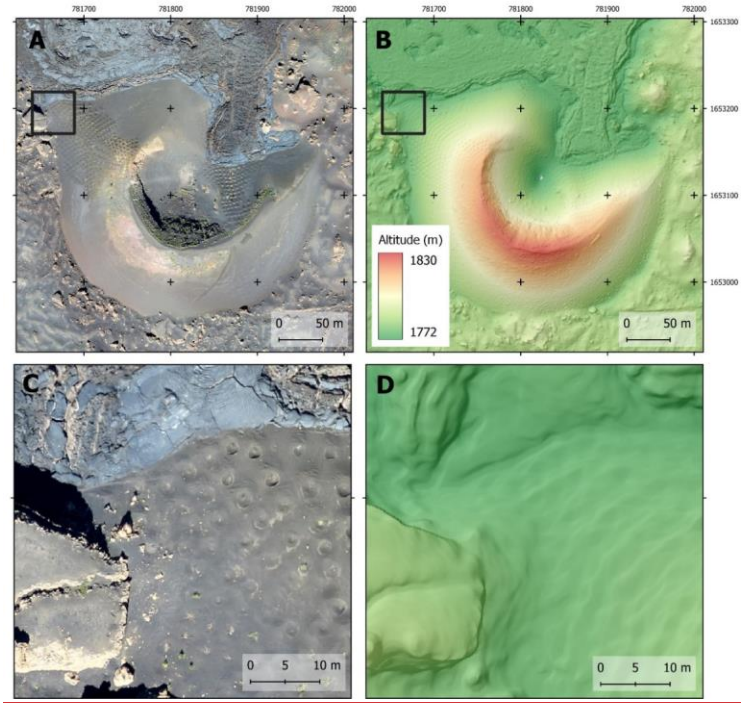

Formatada: Normal, Sem marcas nem numeração

Figure 14 – Examples of the quality of the orthomosaic and DSM of the Chã das Caldeiras in an area of a small volcanic cone. A and C - Orthomosaic (10 cm), B and D – Hill shade model over DSM (10 cm).

Figure 15 shows the ‘a'ā lava flows of 2014-15 close to the village of Portela at two magnifications. It is possible to depict the quality of the survey by viewing the representation of the circular wall structure, as well as the front of the lava lobe present in figures C and D.

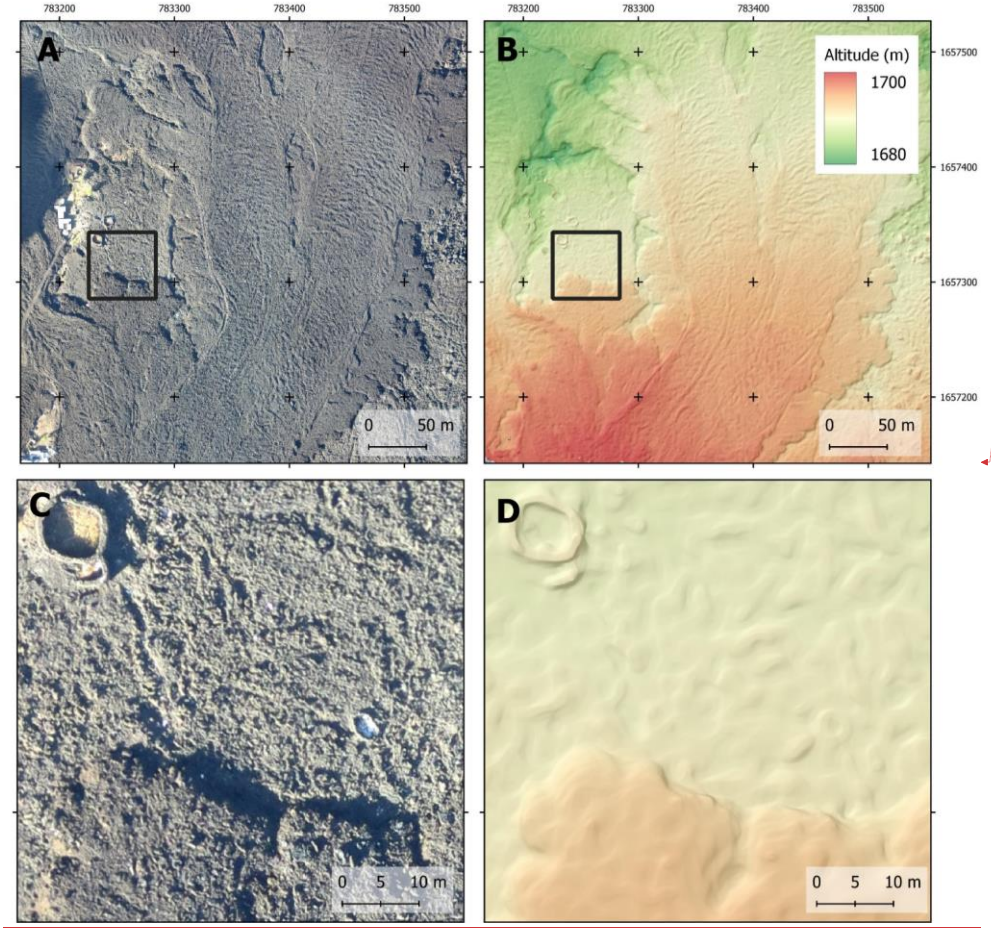

Formatada: Centrado

Figure 15 – Examples of the quality of the orthomosaic and DSM of the Chã das Caldeiras in an area of a ‘a'ā lava flow, showing also a circular wall structure. A and C - Orthomosaic (10 cm), B and D – Hill shade model over DSM (10 cm).

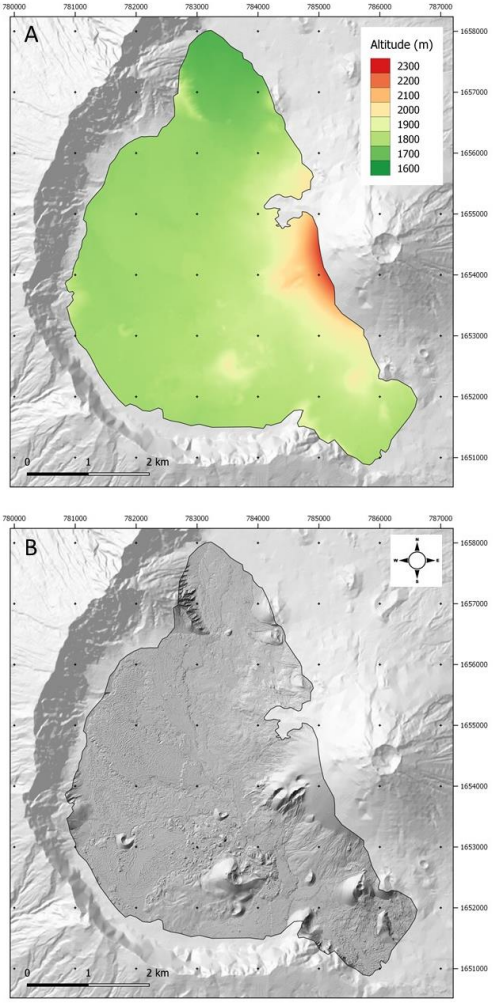

~~Figure 69 – Digital surface model of the Chã das Caldeiras (A) and DSM shaded relief model (B). The surveyed area is overlaying the DEMFI (2010) 5 m DEM.~~

Formatada: Centrado

Formatada: Centrado

The high-quality zones cover 96.8% of the entire survey and coincide with areas of rough surfaces with numerous automatic and manual tie points, where the morphology is very accurate, and the point cloud model has high resolution. Figure 8 10 shows some selected examples of the types of surface present in the survey area, which allow to visually assess the quality of the model outputs.:

- The 'a'ā lava flow fields are characterized by high rugosity and numerous features which are easily matched between aerial photographs, including blocks, frequent sharp slope changes and pressure ridges (Figs. 810 A and 810 B). The
- Pāhoehoe lava flows show a much smoother and homogeneous surface, but they have frequent fractures and lineaments. They occupy generally small sectors of the orthomosaic and are bound by very rough a'ā lavas, facilitating point matching (Figs. 810 C and 810 D). The
- S small volcanic cones with rough surfaces (e.g. boulders, footpaths, lava outcrops) show very high-quality results (Figs. 911 A and 119 B).
- Infrastructure, such as non-paved roads and houses show numerous matches and provide very accurate results. Cultivated areas occupy small sectors of the surveyed area, but the small holes dug to cultivate vines, as well as other small trees, are also very well represented in the DSM (Figs. 911 C and 911 D).

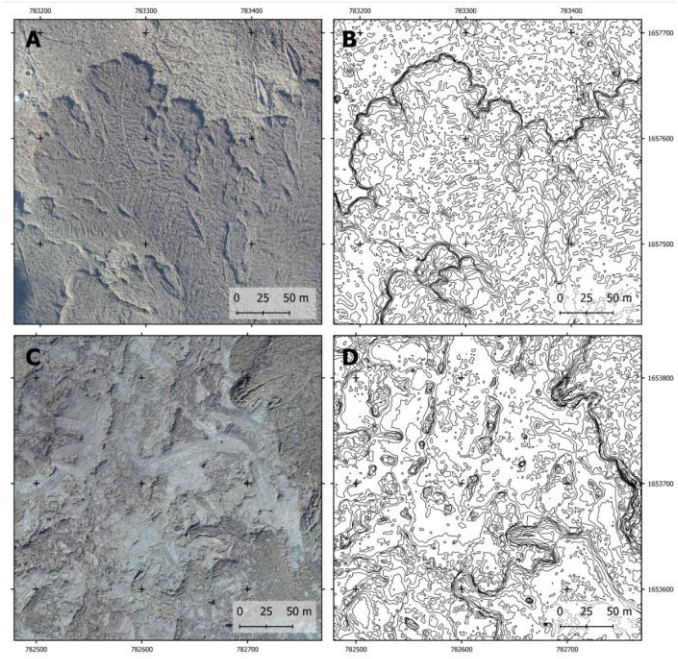

860 **~~Figure 8 10 – Examples of surfaces in the Chã das Caldeiras with high-quality results for the digital surface model, with orthomosaic for visualization (10 cm resolution) and contour lines derived from the digital surface model (50 cm equidistance). Note the good quality of the elevation contours. A and B. 'a'ā lava flows, C and D. Pāhoehoe lava field.~~**

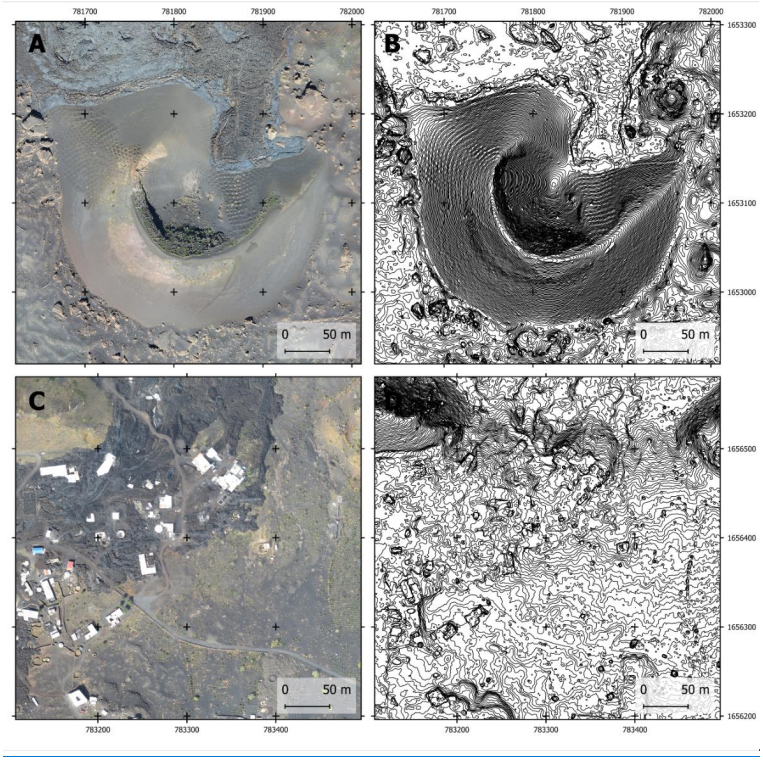

Formatada: Centrado

Formatada: Normal

~~**Figure 119 – Examples of surfaces in the Chã das Caldeiras with high-quality results for the digital surface model, with orthomosaic for visualization (10 cm resolution) and contour lines derived from the digital surface model (50 cm equidistance). Note the good quality of the elevation contours. A and B. Volcanic cone with cultivated areas inside the crater, C and D. Lava field with buildings and a road.**~~

~~The medium-quality zones are sectors dominated by ash and lapilli, where sporadic 3D errors occur and occupy 0.6% of the survey. These areas, which in general can be used for visualization purposes and even for quantification, but with special care. Most errors in these zones are very small (dm scale) and can be smoothed by resampling, for example to 1-2 m resolution (Fig. 1012 A and B).~~ ~~The low-quality zones only occupy 2.6% of the survey area (Fig. 112 C and D). These cases occur in very smooth surfaces of ash and lapilli or in sectors where a small number of overlapping aerial photos exists. They~~

are located mainly in the base of some slopes, concave areas and also in the top of Monte Beco, due to the lack of photo overlapping.

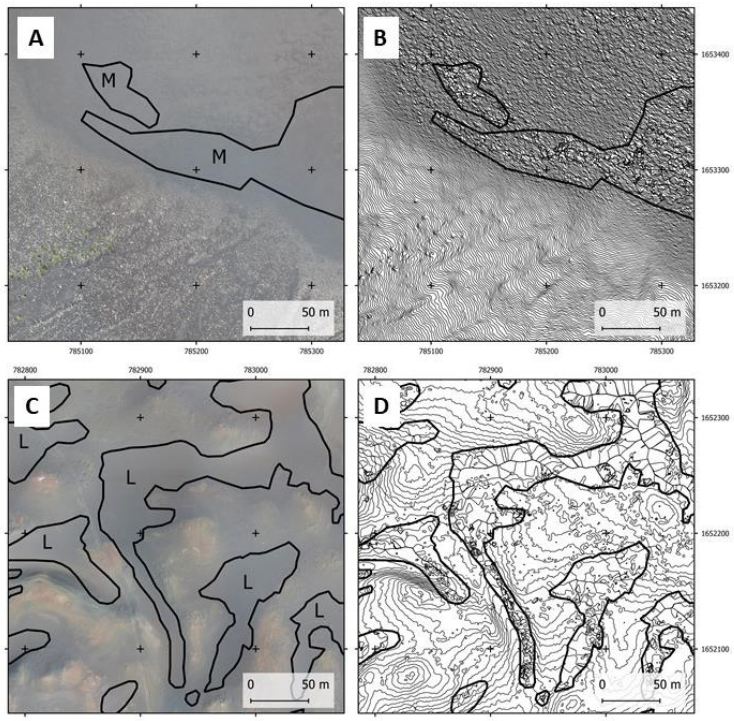

Figure 120 – Examples of surfaces with medium and low quality. A and B: Steep slope covered with ash in the Chã das Caldeiras with medium quality results (M) for the digital surface model. A., with orthomosaic (A, 10 cm resolution), and B. contour lines derived from the digital surface model (B, 50 cm equidistance). The black line shows the boundary of the medium quality area. The contours are very irregular in detail, but the overall slope at a coarse resolution is maintained. The area where the deposits are coarser provides a good DSM. C and D: – Irregular surfaces with linear depressions covered with ash in the Chã das Caldeiras with poorLow quality results (L) for the digital surface model., with A. orothomosaic for visualization (C, 10 cm resolution), and B. contour lines derived from the digital surface model (D, 50 cm equidistance). The black line shows the boundary of the low-quality area. The contours are very irregular and show numerous errors. The border with the good quality areas is sharp with good topography where the ground surface is coarser..

Formatada: Centrado

Formatada: Legenda

~~The low-quality zones correspond to patches where the point cloud was poorly resolved, having numerous artefacts in the DSM (Fig. 11). These areas cannot be used for quantification purposes and their visualization shows errors, which sometimes are significant.~~ The low-quality zones only occupy 2.6% of the survey area (Fig. 11). These cases occur in very smooth surfaces of ash and lapilli or in sectors where a small number of overlapping aerial photos exists. They are located mainly in the base of some slopes, concave areas and also in the top of Monte Beco, due to the lack of photo overlapping.

~~**Figure 11 – Irregular surfaces with linear depressions covered with ash in the Chã das Caldeiras with poor-quality results for the digital surface model. A. orthomosaic for visualization (10 cm resolution), and B. contour lines derived from the digital surface model (50 cm equidistance). The black line shows the boundary of the low-quality area. The contours are very irregular and show numerous errors. The border with the good quality areas is sharp with good topography where the ground surface is coarser.**~~

54.3 Orthophoto mosaic

The digital orthophoto mosaic ~~that shows~~is presented at ~~a~~10 and 25 cm/pixel ~~-~~resolution ~~of 25 cm~~ (Fig. ~~12~~136)~~, but the high accuracy of the survey allowed to make a mosaic with a resolution of 10 cm, which is available in the repository for download. This product may be delivered upon request~~. ~~The mosaic~~It ~~shows an overall high graphic quality~~is especially useful for accurate analysis and mapping at high resolution of small areas. However, when analysed as a whole ~~, with~~it shows ~~few~~ some problems ~~relating~~ associated to shadow effects close to the Bordeira wall in the south of the Chã das Caldeiras, and with varying illumination conditions in the lava flows of the northwest part of the survey, where stri~~p~~ping occurs. These problems only affect the orthomosaic and do not generate changes in quality in the DSM. The sectors with medium quality in the ~~DSM~~point cloud, do not affect the overall quality of the ortho~~-~~mosaic, but areas of low quality may result ~~the interpolation may result~~ in ~~minor~~small geometrical inaccuracies ~~(Fig. 8) in the orthophoto mosaic in the areas of low quality in the DSM~~. This occurs in the areas with very homogeneous ash and lapilli surfaces and the dataset with indication of the quality zones should be checked when detailed analysis are needed.

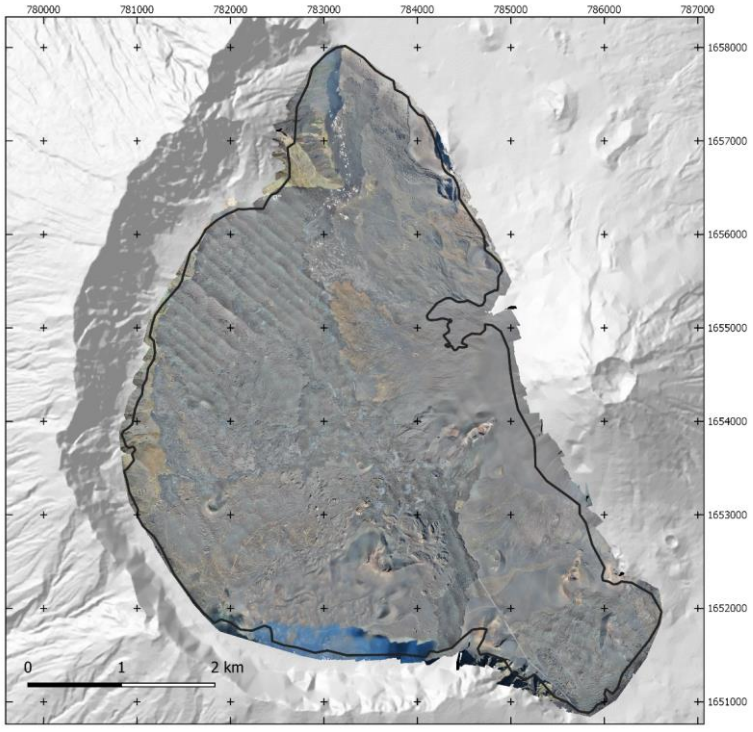

Figure 12~~3~~6 – Digital orthophoto mosaic with 25 cm resolution of the Chã das Caldeiras. ~~The quality of the point cloud is shown in Fig. 7~~The striping results from illumination problems and the artefact in the south is a shadow from the Bordeira wall. The s~~S~~haded relief outside the surveyed area derived from the DEMFI (2010) 5 m DEMFI.

920

5~~4~~.4 3D models for visualization

A 3D texture mesh (.fbx) was produced for visualization purposes, allowing for the accurate visualization of the ~~whole~~ surveyed area (Fig. 14~~7~~3). The file is available in the data set.

Formatada: Centrado

Formatou: Não Realce

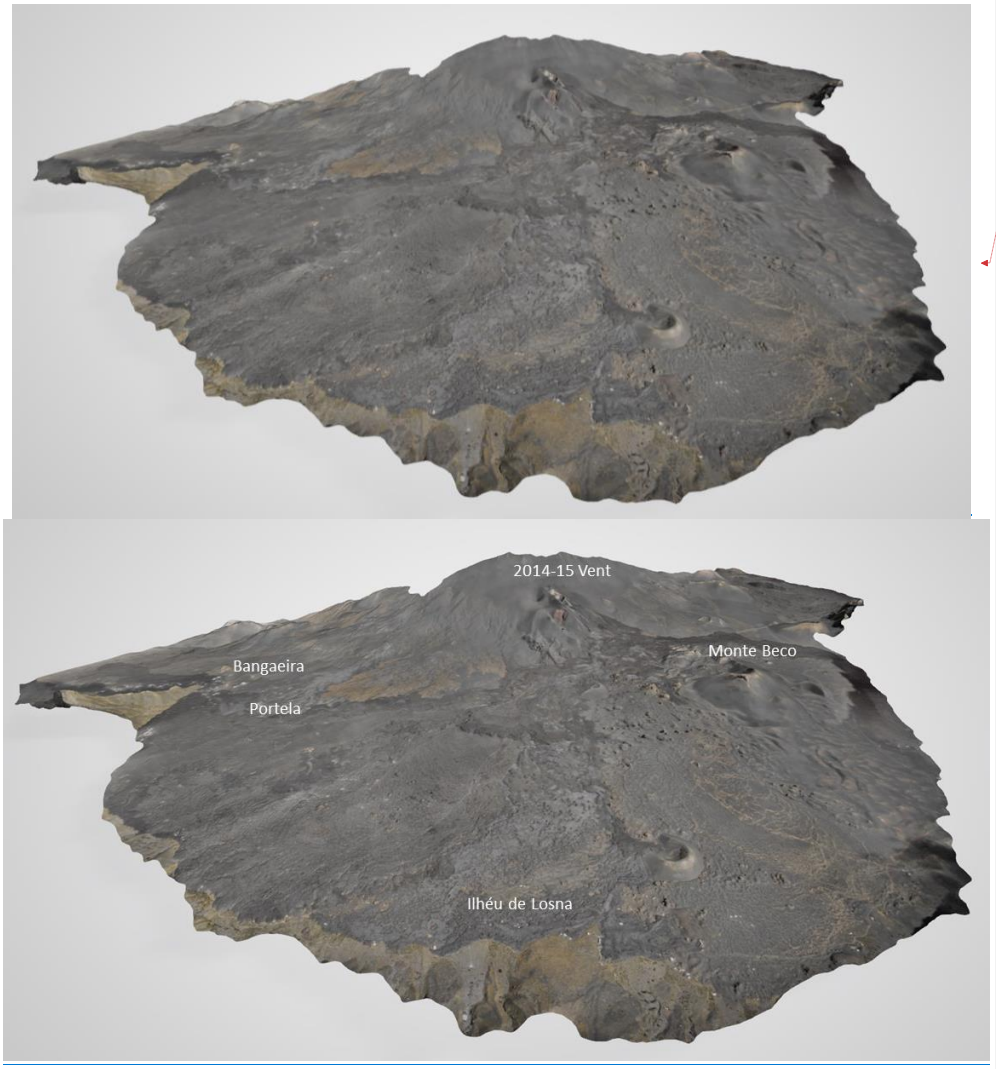

Figure 1743 – 3D visualization of the texture mesh of the Chã das Caldeiras from Ilhéu de Losna towards the east.

Formatada: Centrado

Formatada: Normal

54.5 New estimates of the 2014-15 lava flow field area

~~The lava flow field of the 2014-15 eruption was digitized manually using the orthomosaic and DSM. Unfortunately, our survey missed a small area of the lava flow with 0.007 km² in the northwest sector of Chã das Caldeiras, close to Monte Amarelo and that sector had to be digitised using very high resolution Google Earth imagery.~~ The accuracy of the present survey allowed to calculate a new 2D projected area for the delineation of the 2014-15 lava flow field~~, which~~. The ~~is~~ calculated area is 4.53 km^2, a number smaller than the areas calculated by other authors using coarser resolution ~~imagery~~data, that varied from 4.8 (Bagnardi et al. 2016) to 4.97 km^2 (Bignami et al. 2020) (5.8% to 8.9%). This ~~discrepancy~~ difference ~~can~~ may be explained by the higher spatial resolution of our dataset that allows more accurate delineations, identifying in addition several kīpukas (Fig. 19), ~~i.e. small 'islands' (interior elevations surrounded by lava during the 2014-15 eruption) a~~and also to ~~a~~ the spatial variation effect (Chen, 1999) that results from the computation of the same areas in products with different spatial resolutions.

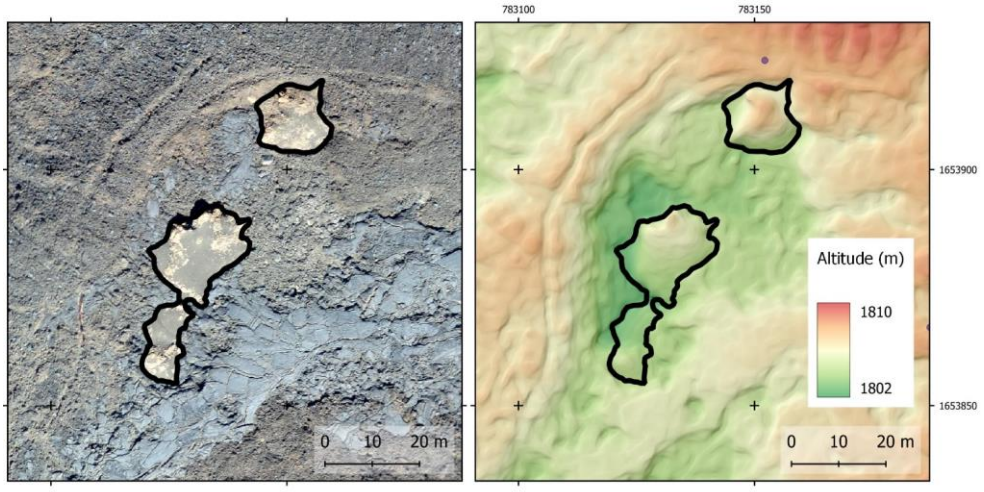

Figure 18 – Example of kīpukas (islands of pre-eruption material surrounded by lava) that have been identified in the present lava delineation, influencing the area estimates when compared to work from other authors. Left: orthomosaic, Right: hill shade model over DSM.

Formatou: Superior à linha

Formatou: Superior à linha

Formatada: Legenda

65. Data availability

The data is available at Zenodo: Vieira, Gonçalo, Mora, Carla, Pina, Pedro, Ramalho, Ricardo, & Fernandes, Rui. (2020). Digital surface model and orthomosaic of the Chã das Caldeiras lava fields (Fogo Island, Cape Verde, December 2016) (Version 11.310.0) [Data set]. Zenodo. http://doi.org/10.5281/zenodo.47185210.5281/zenodo.466770910.5281/zenodo.4035038.

The dataset consists of the following files:

- cha_caldeiras_3d_mesh.fbx: 3D mesh in fbx format.

- cha_caldeiras_contours_50cm.zip: Compressed shapefile (shp) and auxiliary files. Contour lines of the Chã das Caldeiras in December 2016 with 50 cm equidistance, interpolated from the digital surface model. CRS: ESPG 32626 - WGS 84 / UTM Zone 26N, elevation: ellipsoidal ITRF2014 (WGS84).

- cha_caldeiras_dsm_10cm_v2.zip: Compressed Geotiff file. Digital surface model of the Chã das Caldeiras in December 2016 with 10 cm resolution. CRS: ESPG 32626 - WGS 84 / UTM Zone 26N, elevation: ellipsoidal ITRF2014 (WGS84).

- cha_caldeiras_dsm_25cm_v2.tifzip: Compressed Geotiff file. Digital surface model of the Chã das Caldeiras in December 2016 with 25 cm resolution. CRS: ESPG 32626 - WGS 84 / UTM Zone 26N, elevation: ellipsoidal ITRF2014 (WGS84).

- cha_caldeiras_checkpoints.zip: Compressed shapefile (shp) and auxiliary files. Coordinates of the ground control points not included in the modelling and used as check points for accuracy assessment. CRS: ESPG 32626 - WGS 84 / UTM Zone 26N.

- cha_caldeiras_densified_point_cloud.zip: Compressed densified point cloud file (las). CRS: ESPG 32626 - WGS 84 / UTM Zone 26N.

- cha_caldeiras_error_assessment_areas_v2.zip: Compressed shapefile (shp) and auxiliary files. Areas with errors in the point cloud obtained by visual analysis. 1. Low accuracy, 2. Moderate accuracy. CRS: ESPG 32626 - WGS 84 / UTM Zone 26N.

- cha_caldeiras_gcps.zip: Compressed shapefile (shp) and auxiliary files. Coordinates of the ground control points used to georeferenced the model. CRS: ESPG 32626 - WGS 84 / UTM Zone 26N.

- cha_caldeiras_ortho_10cm_v2.zip: Compressed Geotiff file. Orthomosaic RGB of the Chã das Caldeiras in December 2016 with 10 cm resolution. CRS: ESPG 32626 - WGS 84 / UTM Zone 26N, elevation: ellipsoidal ITRF2014 (WGS84).

- cha_caldeiras_ortho_25cm_v2.tif: Orthomosaic RGB of the Chã das Caldeiras in December 2016 with 25 cm resolution. CRS: ESPG 32626 - WGS 84 / UTM Zone 26N.

- cha_caldeiras_pix4d_report.pdf: Report of the processing of the aerial imagery in PIX4D.

- ebee_fogo_projetos.zip: Compressed PIX4D project files (p4d) with the full aerial imagery of the surveys in Chã das Caldeiras.

- lava-2014-15.zip: Compressed shapefile (shp) and auxiliary files. Lava flows of the eruption of 2014-15 digitised from the original 10 cm resolution orthomosaic. CRS: ESPG 32626 - WGS 84 / UTM Zone 26N.

Formatou: Português (Portugal)
Formatou: Português (Portugal)
Formatou: Inglês (Reino Unido)
Formatou: Inglês (Estados Unidos)
Formatou: Inglês (Estados Unidos)
Formatou: Inglês (Estados Unidos)
Formatou: Português (Portugal)
Formatou: Inglês (Estados Unidos)
Formatou: Inglês (Estados Unidos)

7~~6~~. Conclusions

The 23.9 km^2 very high-resolution digital surface model and orthophoto mosaic of the Chã das Caldeiras lava fields developed from UAV surveys of December 2016, show ~~unprecedented~~ very high detail and accuracy ~~(~~, with a resolution ~~resolution =~~of 25 cm and RMSE ~~=~~ of ~~0~~.10.3 c~~m~~). The original models at 10 cm resolution and the imagery data set are also made public available. 96.8% of the survey area has provided a very high-quality DSM, which due to the scarce vegetation and built areas may be used as a DEM. The areas with moderate problems occupy 0.6% of the survey, with only 2.6% of the area showing poor-quality. The sectors with problems in the point cloud and DSM are those associated to very homogeneous ash and lapilli deposits. These areas can be easily masked out of the DSM by using the shapefiles made available in the dataset. The rough surface 'a'ā lavas and the smooth pāhoehoe flows are very accurately determined, as well as the volcanic cones.

The resulting DSM and orthomosaic constitute base datasets ~~of unprecedent detail~~ of high-value for Earth System Science, e.g. ~~geological research and~~ for lava flow modelling, baseline for future eruptive activity, for studying hydrological changes, ecological recolonisation of lava flows, planning and ~~with a high potential for applications in~~ risk mitigation, among others. The~~se~~ products allow delineating accurately the borders between different surfaces (lava types and other classes) and perceiving sub-meter surface features, which is less accurate or not achievable at all at meter scale, over an area of several square kilometres. These ~~morphometrics~~ features include pressure ridges, tumuli, flow channels, levées, dragged blocks and remains of human structures, among other smaller features such a vegetation.

~~Finally, we consider that t~~These highly detailed products can play a relevant role in the assessment of volcanic hazards and related research ~~and whose importance is surely excelled by becoming open access~~.

Acknowledgements

This research was conducted in the framework of the project FIRE – Fogo Island Volcano: multidisciplinary research on the 2014 eruption (FCT - PTDC/GEO-GEO/1123/2014) funded by the Fundação para a Ciência e a Tecnologia. R. Ramalho acknowledges his IF/01641/2015 contract funded by FCT. The project 3DAntártida funded the acquisition of the UAV. The INGT – Instituto Nacional de Gestão do Território and INMG – Instituto Nacional de Meteorologia e Geofísica de Cabo Verde are thanked for their cooperation. Pedro Almeida, Carla Candeias, Stéphanie Dumont, Bento Martins and Carlos Oliveira are thanked for their support in the collection of ground control points. Carlos Oliveira, Bruno Faria, Euda Miranda, Fátima Fernandes and Jair Rodrigues are thanked for their support to the project and field activities. Co-funding by FCT I.P. UIDB/00295/2020 – CEG and UIDP/00295/2020 - CEG, FCT - UIDB/50019/2020 – IDL and C4G – POCI-01-0145-FEDER-022151. The reviews by the referees Bianca Wagner, Moritz Kirsch, Pablo J. Gonzalez and Samuel Thiele, and the public interactive comment by Gaia Stucky de Quay, provided very welcome and thorough reviews to the original manuscript, which significantly contributed to its final form. We thank them for the detailed commentaries.

Author contributions

GV, CM, PP and RR prepared the UAV survey planning and wrote the manuscript. GV and CM conducted the UAV surveys. PP and RR ~~conducted~~ handled the GNSS GCP collection. GV and CM ~~conducted~~ did the modelling. RR digitised the lava flows. RF coordinated the GNSS activities. All authors contributed to discussion and review of the manuscript.

References

~~Amici, S., Turci, M., Giammanco, S., Spampinato, L., and Giulietti, F.: UAV thermal infrared remote sensing of an Italian mud volcano, Adv. Remote Sens, 02, 04, 358–364, http://dx.doi.org/10.4236/ars.2013.24038, 2013.~~

Bagnardi, M., Gonzàlez, P. J., and Hooper, A.: High-resolution digital elevation model from tri-stereo Pleiades-1 satellite imagery for lava flow volume estimates at Fogo volcano: tri-stereo Pleiades DEM of Fogo volcano, Geophysical Research Letters 43, http://dx.doi.org/10.1002/2016GL069457~~http://dx.doi.org/10.1002/2016GL06945~~, 2016.

Baldi, P., Bonvalot, S., Briole, P., Coltelli, M., Gwinner, K., Marsella, M., Puglisi, G., and Rémy, D.: Validation and comparison of different techniques for the derivation of digital elevation models and volcanic monitoring (Vulcano Island, Italy), Int. J. Remote Sens., 23, 22, 4783–4800. https://doi.org/10.1080/01431160110115861, 2002.

Barrett, R., Lebas, E., Ramalho, R., Klaucke, I., Kutterolf, S., Klügel, A., Lindhorst, K., Gross, F., and Krastel, S.: Revisiting the tsunamigenic volcanic flank-collapse of Fogo Island in the Cape Verdes, offshore West Africa. Geological Society, London, Special Publications, 500, https://doi.org/10.1144/SP500-2019-187, 2019.

Bebiano, J.: A geologia do arquipélago de Cabo Verde. Comunicações dos Serviços Geológicos de Portugal, 18, 167–187, 1932.

~~Benoit, L., Gourdon, A., Vallat, R., Irarrazaval, I., Gravey, M., Lehmann, B., Prasicek, G., Gräff, D., Herman, F., and Mariethoz, G.: A high-resolution image time series of the Gorner Glacier – Swiss Alps – derived from repeated unmanned aerial vehicle surveys, Earth Syst. Sci. Data, 11, 579–588, https://doi.org/10.5194/essd-11-579-2019, 2019.~~

Bignami, C., Chini, M., Amici, S. and Trasatti E.: Synergic use of multi-sensor satellite data for volcanic hazards monitoring: the Fogo (Cape Verde) 2014-2015 effusive eruption, Frontiers of Earth Science, 8, 22, https://doi.org/10.3389/feart.2020.00022, 2020.

~~Bonali, F. L., Tibaldi, A., Marchese, F., Fallati, L., Russo, E., Corselli, C., and Savini, A.: UAV-based surveying in volcano-tectonics: An example from the Iceland rift, Journal of Structural Geology, 121, 46–64, https://doi.org/10.1016/j.jsg.2019.02.004, 2019.~~

Brum da Silveira, A., Madeira, J., and Serralheiro, A.: A estrutura da Ilha do Fogo, Cabo Verde. A Erupção Vulcânica de 1995 na Ilha do Fogo, Cabo Verde. Publ. IICT, Lisboa, 63–78, 1997a.

Brum da Silveira, A., Madeira, J., Serralheiro, A., Torres, P.C., Silva, L.C., and Mendes, M. H.: O controlo estrutural da erupção de Abril de 1995 na Ilha do Fogo, Cabo Verde. A Erupção Vulcânica de 1995 na Ilha do Fogo, Cabo Verde. Publ. IICT, Lisboa, 51–61, 1997b.

Brunier, G., Fleury, J., Anthony, E. J., Gardel, A., and Dussouillez, P.: Close-range airborne Structure-from-Motion Photogrammetry for high-resolution beach morphometric surveys: Examples from an embayed rotating beach, Geomorphology, 261, 76–88, http://doi.org/10.1016/j.geomorph.2016.02.025, 2016.

Bühler, Y., Adams, M. S., Bösch, R., and Stoffel, A.: Mapping snow depth in alpine terrain with unmanned aerial systems (UAS): potential and limitations. The Cryosphere, 10, 1075-1088, https://doi.org/10.5194/tc-10-1075-2016, 2016.

Burke, K., and Wilson, J.T.: Is the African plate stationary? Nature, 239, 5372, 387-390, https://doi.org/10.1038/239387b0 ,1972.

Campana, S.: Drones in Archaeology. State-of-the-art and Future Perspectives, Archaeol. Prospect, 24, 275–296, https://doi.org/10.1002/arp.1569, 2017.

Cappello, A., Ganci, G., Calvari, S., Pérez, N. M., Hernández, P. A., Silva, S. V., Cabral, J., and Negro, C. D.: Lava flow hazard modeling during the 2014–2015 Fogo eruption, Cape Verde, Journal of Geophysical Research: Solid Earth, 121, 2290–2303, https://doi.org/10.1002/2015JB012666, 2016.

Chikhradze, N., Henriques, R., Elashvili, M., Kirkitadze, G., Janelidze, Z., Bolashvili, N., and Lominadze, G.: Close Range Photogrammetry in the Survey of the Coastal Area Geoecological Conditions (on the Example of Portugal), 4, 35–40, http://doi.org/10.11648/j.earth.s.2015040501.17, 2015.

Chio, S.-H. and Lin, C.-H.: Preliminary study of UAS equipped with thermal camera for volcanic geothermal monitoring in Taiwan, Sensors, 17, 1649, https://doi.org/10.3390/s17071649, 2017.

Christiansen, P., Steen, K. A., Jorgensen, R. N., and Karstoft, H.: Automated detection and recognition of wildlife using thermal cameras, Sensors, 14, 13778–13793, https://doi.org/10.3390/s140813778, 2014.

Colomina, I. and Molina, P.: Unmanned aerial systems for photogrammetry and remote sensing: A review, ISPRS Journal of Photogrammetry and Remote Sensing, 92, 79–97, http://dx.doi.org/10.1016/j.isprsjprs.2014.02.013, 2014.

Dąbski, M., Zmarz, A., Rodzewicz, M., Korczak-Abshire, M., Karsznia, I., Lach, K., Rachlewicz, G., and Chwedorzewska, K.: Mapping glacier forelands based on UAV BVLOS operation in Antarctica, Remote Sensing, 12 ,4, 630, https://doi.org/10.3390/rs12040630, 2020.

Darmawan, H., Walter, T. R., Brotopuspito, K. S.,Subandriyo, and Nandaka, I. G. M. A.: Morphological and structural changes at the Merapi lava dome monitored in 2012–15 using unmanned aerial vehicles (UAVs), Journal of Volcanology and Geothermal Research, 349, 256-267. https://doi.org/10.1016/j.jvolgeores.2017.11.006, 2018.

Day, S. J., Heleno, S. I. N., and Fonseca, J. F. B. D.: A past giant lateral collapse and present-day flank instability of Fogo, Cape Verde Islands. Journal of Volcanology and Geothermal Research, 94, 191-218, https://doi.org/10.1016/S0377-0273(99)00103-1, 1999.

De Beni, E., Cantarero, M., and Messina, A.: UAVs for volcano monitoring: A new approach applied on an active lava flow on Mt. Etna (Italy), during the 27 February–02 March 2017 eruption, Journal of Volcanology and Geothermal Research, 369, 250–262, https://doi.org/10.1016/j.jvolgeores.2018.12.001, 2019.

de Moor, J. M., Stix, J., Avard, G., Muller, C., Corrales, E., Diaz, J. A., Alan, A., Brenes, J., Pacheco, J., Aiuppa, A., and Fischer, T. P.: Insights on hydrothermal-magmatic interactions and eruptive processes at Poás volcano (Costa Rica) from high frequency gas monitoring and drone measurements, Geophysical Research Letters, 46, 1293–1302, https://doi.org/10.1029/ 2018GL08030, 2019.

Di Felice, F., Mazzini, A., Di Stefano, G., and Romeo, G.: Drone high resolution infrared imaging of the Lusi mud eruption, Marine and Petroleum Geology, 90, 38–51, http://dx.doi.org/10.1016/j.marpetgeo.2017.10.025, 2018.

Diefenbach, A. K., Bull, K. F., Wessels, R. L., and McGimsey, R. G.: Photogrammetric monitoring of lava dome growth during the 2009 eruption of Redoubt Volcano, J. Volcanol. Geotherm. Res., 259, 308–316, https://doi.org/10.1016/j.jvolgeores.2011.12.009, 2013.

Eisele, S., Reißig, S., Freundt, A., Kutterolf , S., Nürnberg, D., Wang, K.L., and Kwasnitschka, T.: Pleistocene to Holocene offshore tephrostratigraphy of highly explosive eruptions from the southwestern Cape Verde Archipelago, Marine Geology, 369, 233-250, https://doi.org/10.1016/j.margeo.2015.09.006, 2015.

Faria, B. and Fonseca, J. F. B. D.: Investigating volcanic hazard in Cape Verde Islands through geophysical monitoring: network description and first results, Natural Hazards and Earth System Sciences, 14, 485–499, https://doi.org/10.5194/nhess-14-485-2014, 2014.

Favalli, M., Fornaciai, A., Nannipieri, L., Harris, A., Calvari, S., and Lormand C.: UAV-based remote sensing surveys of lava flow fields: a case study from Etna's 1974 channel-fed lava flows, Bulletin of Volcanology, 80, 29. https://doi.org/10.1007/s00445-018-1192-6, 2018.

Favalli, M., Fornaciai, A., and Pareschi, M.T.: LIDAR strip adjustment: Application to volcanic areas, Geomorphology, 111, 3, 123–135, https://doi.org/10.1016/j.geomorph.2009.04.010, 2009.

Fonseca, J., Flor, A., Goncalves, A., Day, S., Jenkyns, S.: Perigosidade vulcânica das ilhas de Cabo Verde, in: Riscos geológicos das ilhas de Cabo Verde, Municipia Final Report to Cape Verde UNDP Office, edited by Mileu, N., Lisbon, 2014.

Fornaciai, A., Bisson, M., Landi, P., Mazzarini, F., and Pareschi, M.T.: A LiDAR survey of Stromboli volcano (Italy): Digital elevation model-based geomorphology and intensity analysis, Int. J. Remote Sens., 31, 12, 3177–3194, https://doi.org/10.1080/01431160903154416, 2010.

Gomez, C. and Purdie, H.: UAV- based photogrammetry and geocomputing for hazards and disaster risk monitoring – A review, Geoenvironmental Disasters, 3, 23, http://doi.org/10.1186/s40677-016-0060-y, 2016.

González, P. J., Bagnardi, M., Hooper, A.J., and Larsen, Y., Marinkovic, P., Samsonov, S.V., Wright, T.J.: The 2014–2015 eruption of Fogo volcano: Geodetic modeling of Sentinel-1 TOPS interferometry, Geophysical Research Letters, 42, 21, 9239-9246, https://doi.org/10.1002/2015GL066003 2015.

Hassan-Esfahani, L., Torres-Rua, A., Jensen, A., and McKee, M.: Assessment of surface soil moisture using high-resolution multi-spectral imagery and artificial neural networks, Remote Sens., 7, 2627–2646, https://doi.org/10.3390/rs70302627, 2015.

Hassler, S. C. and Baysal-Gurel, F.: Unmanned Aircraft System (UAS) technology and applications in agriculture, Agronomy, 9, 618, https://doi.org/10.3390/agronomy9100618, 2019.

Heleno da Silva, S.I.N., Day, S.J., and Fonseca, J.F.B.D.: Fogo Volcano, Cape Verde Islands: seismicity-derived constraints on the mechanism of the 1995 eruption, J. Volcanol. Geotherm. Res., 94, 219–231, https://doi.org/10.1016/S0377-0273(99)00104-3, 1999.

James, M.R., Chandler, J.H., Eltner, A., Fraser, C., Miller, P.E., Mills, J.P., Noble, T., Robson, S., and Lane, S.N., Guidelines on the use of structure-from-motion photogrammetry in geomorphic research. Earth Surf. Process. Landforms, 44: 2081– 2084. https://doi.org/10.1002/esp.4637, 2019.

James, M. R., Carr, B., D'Arcy, F., Diefenbach, A., Dietterich, H., Fornaciai, A., Lev, E., Liu, E., Pieri, D., Rodgers, M., Smets, B., Terada, A., von Aulock, F., Walter, T., Wood, K. and Zorn, E., Volcanological applications of unoccupied aircraft systems (UAS): Developments, strategies, and future challenges", Volcanica 3(1), 67–114. doi: 10.30909/vol.03.01.67114.

Jenkins, S. F., Day, S. J., Faria, B.V.E., and Fonseca, J. F. B. D.: Damage from lava flows: insights from the 2014–2015 eruption of Fogo, Cape Verde, Journal of Applied Volcanology, 6, 1, 1-17, https://doi.org/10.1186/s13617-017-0057-6, 2017.

Jordan, B.R.: Collecting field data in volcanic landscapes using small UAS (sUAS)/drones, Journal of Volcanology and Geothermal Research, 385, 231–241, https://doi.org/10.1016/j.jvolgeores.2019.07.006, 2019.

Jouvet, G., Dongen, E., Lüthi, M.P., and Vieli, A.: In situ measurements of the ice flow motion at Eqip Sermia Glacier using a remotely controlled unmanned aerial vehicle (UAV), Geosci. Instrum. Method. Data Syst., 9, 1–10, https://doi.org/10.5194/gi-9-1-2020, 2020.

Kattenborn, T., Sperlich, M., Bataua, K., and Koch, B.: Automatic Single Tree Detection in Plantations using UAV-based Photogrammetric Point clouds. ISPRS – International Archives of the Photogrammetry, Remote Sensing and Spatial Information Sciences, XL- 3(September), 139–144. http://doi.org/10.5194/isprsarchives-XL-3-139-2014, 2014.

Kerle, N.: Volume estimation of the 1998 flank collapse at Casita volcano, Nicaragua: A comparison of photogrammetric and conventional techniques, Earth Surf. Processes Landforms, 27, 7, 759–772, https://doi.org/10.1002/esp.351, 2002.

Komorowski, J. C., Morin, J., Jenkins, S., and Kelman, I.: Challenges of Volcanic Crises on Small Islands States. In: Fearnley C.J., Bird D.K., Haynes K., McGuire W.J., Jolly G. (eds) Observing the Volcano World. Advances in Volcanology (An Official Book Series of the International Association of Volcanology and Chemistry of the Earth's Interior – IAVCEI, Barcelona, Spain). Springer, https://doi.org/10.1007/11157_2015_15, 2016.

Küng, O., Strecha, C., Beyeler, A., Zufferey, J-C., Floreano, D., Fua, P., and Gervaix, F: The Accuracy of Automatic Photogrammetric Techniques on Ultra-light UAV Imagery. International Archives of the Photogrammetry, Remote Sensing and Spatial Information Sciences - ISPRS Archives. 38. https://doi.org/10.5194/isprsarchives-XXXVIII-1-C22-125-2011, 2011.

Le Bas, T. P., Masson, D.G., Holtom, R. T. and Grevemeyer, I.: Slope failures of the flanks of the southern Cape Verde Islands. In: Lykousis, V., Sakellariou, D. and Locat, J. (eds) Submarine Mass Movements and Their Consequences.

Formatou: Tipo de letra: Não Itálico

Formatou: Inglês (Reino Unido)

Formatou: Inglês (Reino Unido)

Formatou: Inglês (Reino Unido)

Formatou: Inglês (Reino Unido)

Código de campo alterado

Advances in Natural and Technological Hazards Research, 27. Springer, Dordrecht, 337–345, https://doi.org/10.1007/978-1-4020-6512-5_35, 2007.

Lindgren, P. R., Grosse, G., Walter, Anthony K. M., and Meyer, F. J.: Detection and spatiotemporal analysis of methane ebullition on thermokarst lake ice using high-resolution optical aerial imagery, Biogeosciences, 13, 27-44, https://doi.org/10.5194/bg-13-27-2016, 2016.

Liu, E.J., Wood, K., Mason, E., Edmonds, M., Aiuppa, A., Giudice, G., Bitetto, M., Francofonte, V., Burrow, S., Richardson, T., Watson, M., Pering, T. D., Wilkes, T.C., McGonigle, A. J. S., Velasquez, G., Melgarejo, C., and Bucarey C.: Dynamics of outgassing and plume transport revealed by proximal unmanned aerial system (UAS) measurements at Volcán Villarrica, Chile. Geochemistry, Geophysics, Geosystems, 20, 730–750, https://doi.org/10.1029/2018GC007692, 2019.

Lodge, A. and Helffrich, G.: Depleted swell root beneath the Cape Verde Islands, Geology, 34, 6, 449-452, https://doi.org/10.1130/G22030.1, 2006.

Long, N., Millescamps, B., Guillot, B., Pouget, F, and Bertin, X.: Monitoring the Topography of a Dynamic Tidal Inlet Using UAV Imagery, Remote Sens., 8, 387, https://doi.org/10.3390/rs8050387, 2016.

Lucieer, A., de Jong, S. M., and Turner, D.: Mapping landslide displacements using Structure from Motion (SfM) and image correlation of multi-temporal UAV photography, Progress in Physical Geography, 38, 1, 97–116. http://doi.org/10.1177/0309133313515293, 2014.

Machado, F. and Torre de Assunção, C. F.: Carta geológica de Cabo Verde na escala de 1/100,000.; noticia explicativa da folha da ilha do Fogo — estudos petrográficos. Garcia de Orta, Lisboa. 13, 597–604, 1965.

Madeira, J., Brum da Silveira, A., Mata, J., Mourão, C., and Martins, S.: The role of mass movements on the geomorphologic evolution of island volcanoes: examples from Fogo and Brava in the Cape Verde archipelago, Comunicações Geológicas, 95, 93–106, 2008.

Madeira, J., Ramalho, R. S., Hoffmann, D. L., Mata, J., and Moreira, M.: A geological record of multiple Pleistocene tsunami inundations in an oceanic island: The case of Maio, Cape Verde, Sedimentology, 67, 1529–1552, https://doi.org/10.1111/sed.12612, 2020.

Major, J.J., Dzurisin, D., Schilling, S. P., and Poland, M. P.: Monitoring lava-dome growth during the 2004–2008 Mount St. Helens, Washington, eruption using oblique terrestrial photography, Earth Planet. Sci. Lett., 286, 1–2, 243–254, https://doi.org/10.1016/j.epsl.2009.06.034, 2009.

Masson, D.G., Le Bas, T. P., Grevemeyer, I., and Weinrebe, W.: Flank collapse and large-scale landsliding in the Cape Verde Islands, off West Africa, Geochemistry, Geophysics, Geosystems, 9, 16, https://doi.org/10. 1029/2008GC001983, 2008.

Mata, J., Martins, S., Mattielli, N., Madeira, J., Faria, B., Ramalho, R., Silva, P., Moreira, M., Caldeira, R., Moreira, M., Rodrigues, J., and Martins, L.: The 2014–15 eruption and the short-term geochemical evolution of the Fogo volcano (Cape Verde): Evidence for small-scale mantle heterogeneity, Lithos, 288-289, 91-107, https://doi.org/10.1016/j.lithos.2017.07.001, 2017.

Formatou: Português (Portugal)

Mazzarini, F. M. T. Pareschi, M. Favalli, I. Isola, S. Tarquini, and E. Boschi.: Lava flow identification and aging by means of lidar intensity: Mount Etna case, J. Geophys. Res., 112, B02201, https://doi.org/10.1029/2005JB004166, 2007.

McGonigle, A. J. S., Aiuppa, A., Giudice, G., Tamburello, G., Hodson, A.J., and Gurrieri, S.: Unmanned aerial vehicle measurements of volcanic carbon dioxide fluxes, Geophys. Res. Lett., 35, 6, L06303, https://doi.org/10.1029/2007GL032508, 2008.

Miranda, V., Pina, P., Heleno, S., Vieira, G., Mora, C., and Schaefer, C. E. G. R.: Monitoring recent changes of vegetation in Fildes Peninsula (King George Island, Antarctica) through satellite imagery guided by UAV surveys, Science of The Total Environment, 704, 135295, https://doi.org/10.1016/j.scitotenv.2019.135295, 2020.

Mora, C., Vieira, G., Pina, P., Lousada, M., and Christiansen, H. H.: Land Cover Classification Using High Resolution Aerial Photography in Adventdalen, Svalbard, Geografiska Annaler: Series A, Physical Geography, 97, 3, 473-488, http://doi.org/10.1111/geoa.12088, 2015.

Mori, T., Hashimoto, T., Terada, A., Yoshimoto, M., Kazahaya, R., Shinohara, H., and Tanaka, R.: Volcanic plume measurements using a UAV for the 2014 Mt. Ontake Eruption, Earth Planets Space, 68–49, https://doi.org/10.1186/s40623-016-0418-0, 2016.

Mouginis-Mark, P. J., and Garbeil, H.: Quality of TOPSAR topographic data for volcanology studies at Kılauea Volcano, Hawaii: An assessment using airborne lidar data, Remote Sens. Environ., 96, 2, 149–164, https://doi.org/10.1016/j.rse.2005.01.017, 2005.

Müller, D., Walter, T.R., Schöpa, A., Witt, T., Steinke, B., Gudmundsson, M.T., and Dürig, T.: High-resolution digital elevation modeling from TLS and UAV campaign reveals structural complexity at the 2014/2015 Holuhraun eruption site, Iceland, Front. Earth Sci., 5, 59, https://doi.org/10.3389/feart.2017.00059, 2017.

Nakano, T., Kamiya, I., Tobita, M., Iwahashi, J., and Nakajima, H.: Landform monitoring in active volcano by UAVand SfM-MVS technique. The International Archives of the Photogrammetry, Remote Sensing and Spatial Information Sciences, 40, 8, 71–75, https:// doi.org/10.5194/isprsarchives-XL-8-71-2014 , 2014.

Pajares, G.: Overview and current status of remote sensing applications based on Unmanned Aerial Vehicles (UAVs), Photogrammetric Engineering & Remote Sensing, 81,4, 281-330, https://doi.org/10.14358/PERS.81.4.281, 2015.

Paris, R., Geichetti, T., Chevalier, J., Guillou, H., and Frank, N.: Tsunami deposits in Santiago Island (Cape Verde archipelago) as possible evidence of a massive flank failure of Fogos volcano, Sedimentary Geology, 239, 129–145, https://doi.org/10.1016/j.sedgeo. 2011.06.006, 2011.

Paris, R., Ramalho, R.S., Madeira, J., Ávila, S., May, S.M., Rixhon, G., Engel, M., Brückner, H., Herzog, M., Schukraft, G., and Perez-Torrado, F.J.: Mega-tsunami conglomerates and flank collapses of ocean island volcanoes, Marine Geology, 395, 168-187, https://doi.org/10.1016/j.margeo.2017.10.004, 2018.

Poland, M.P.: Time-averaged discharge rate of subaerial lava at K¯ılauea Volcano, Hawai'i, measured from TanDEM-X interferometry: Implications for magma supply and storage during 2011–2013, J. Geophys. Res. Solid Earth, 119, 5464–5481, https://doi.org/10.1002/2014JB011132, 2014.

Ramalho, R., Winckler, G., Madeira, J., Helffrich, G. Hipólito, A., Quartau, R., Adena, K., and Schaefer, J.: Hazard potential of volcanic flank colapses raised by new megatsunami evidence, Science Advances, 1, 9, E1500456, https://doi.org/10.1126/sciadv.1500456, 2015.

Ramalho, R. A. S. (Ed.): Building the Cape Verde Islands, 1st ed., Springer, Berlin, Heidelberg, 2011.

Ramalho, R, Helffrich, D., Cosca, M.,Vance, D, Hoffmann, D., and Schmidt, D. N.: Episodic swell growth inferred from variable uplift of the Cape Verde hotspot islands, Nature Geoscience, 3, 11, 774–777, https://doi.org/10.1038/ngeo982, 2010a.

Ramalho, R., Helffrich, D., Cosca, M., Vance, D., Hoffmann, D., and Schmidt, D. N.: Vertical movements of ocean island volcanoes: Insights from a stationary plat. environment, Marine Geology., 275, 84–95, https://doi.org/10.1016/j.margeo.2010.04.009, 2010b.

Ramalho, R. S., Helffrich, G., Schmidt, D. N., and Vance, D.: Tracers of uplift and subsidence in the Cape Verde Archipelago, Journal of the Geological Society of London, 167, 3, 519–538, doi:10.1144/0016 -76492009-056, 2010c.

Ribeiro, O.: A ilha do Fogo e as suas erupções. Comissão Nacional para as Comemorações dos Descobrimentos Portugueses, 1954.

Richter, N., Favalli, M., Dalfsen, E. Z., Fornaciai, A., Fernandes, R. M. S., Rodriguez, N. P., Levy, J., Victória, S. S., and Walter, Th.R.: Lava flow hazard at Fogo volcano, Cape Verde, before and after the 2014–2015 eruption, Natural Hazards and Earth Systems, 16, 1925–1951, https://doi.org/10.5194/nhess-16-1925-2016, 2016.

~~Risbøl, O. and Gustavsen, L.: LiDAR from drones employed for mapping archaeology – Potential, benefits and challenges, Archaeological Prospection, 25, 4, 329-338, https://doi.org/10.1002/arp.1712, 2018.~~

Rowland, S. K., MacKay, M.E., Garbeil, H., and Mouginis-Mark, P. J.: Topographic analyses of K¯ılauea Volcano, Hawai'i, from interferometric airborne radar, Bull. Volcanol., 61, 1–2, 1–14, doi:10.1029/2019GL083501, 1999.

~~Rüdiger, J., Tirpitz, J. L., de Moor ,J.M., Bobrowski, N., Gutmann, A., Liuzzo, M., Ibarra ,M., and Hoffmann, T.: Implementation of electrochemical, optical and denuder-based sensors and sampling techniques on UAV for volcanic gas measurements: examples from Masaya, Turrialba and Stromboli volcanoes, Atmospheric Measurement Techniques, 11, 2441–2457, https://doi.org/10.5194/amt-11-2441-2018, 2018.~~

~~Salzer, J. T., Milillo, P., Varley, N., Perissin, D., Pantaleo, M., and Walter, T. R.: Evaluating links between deformation, topography and surface temperature at volcanic domes: results from a multi-sensor study at Volcán de Colima, Mexico, Earth Planet. Sci. Lett. 479, 354–365, https://doi.org/10.1016/j.epsl.2017.09.027, 2017.~~

Smith, M. W., Carrivick, J .L., and Quincey, D. J.: Structure from motion photogrammetry in physical geography, Progress in Physical Geography, 40, 2, 247–275, https://doi.org/10.1016/j.geomorph.2012.08.021, 2016.

Stevens, N., Wadge, G., and Murray, J.: Lava flow volume and morphology from digitised contour maps: A case study at Mount Etna, Sicily, Geomorphology, 28, 3–4, 251–261, https://doi.org/10.1016/S0169-555X(98)00115-9, 1999.

Stix, J., de Moor, J .M., Rüdiger, J., Alan, A., Corrales, E., D'Arcy, F., Diaz, J. A., and Liotta, M.: Using drones and miniaturized instrumentation to study degassing at Turrialba and Masaya volcanoes, Central America, Journal of Geophysical Research: Solid Earth, 123, 6501–6520, https://doi.org/10.1029/2018JB015655, 2018.

Thiele, S. T., Varley, N., and James, M. R.: Thermal photogrammetric imaging: a new technique for monitoring dome eruptions, J. Volcanol. Geotherm. Res., 337, 140–145, https://doi.org/10.1016/j.jvolgeores.2017.03.022, 2017.

Torres, P. C., Madeira, J., Silva, L. C., Brum da Silveira, A., Serralheiro, A., and Mota Gomes, A.: Carta Geológica das Erupções Históricas da Ilha do Fogo (Cabo Verde): revisão e actualização, Comunicações do Instituto Geológico e Mineiro 84, A193–196, 1998.

Turner, N. R., Perroy, R. L., and Hon, K.: Lava flow hazard prediction and monitoring with UAS: a case study from the 2014–2015 Pāhoa lava flow crisis, Hawai'I, Journal of Applied Volcanology, 6,17. http://doi.org/10.1186/s13617-017-0068-3, 2017.

Vieira, D., Teodoro, A., and Gomes, A.: Analysing Land Surface Temperature variations during Fogo Island (Cape Verde) 2014-2015 eruption with Landsat 8 images, Proc. of SPIE, 10005, 1000508-14, 2016.

Vieira, G., Mora, C., Pina, P., Ramalho, R., and Fernandes, R.: Digital surface model and orthomosaic of the Chã das Caldeiras lava fields (Fogo Island, Cape Verde, December 2016) (Version 1.03.0) [Data set]. Zenodo. http://doi.org/10.5281/zenodo.4718520http://doi.org/10.5281/zenodo.4035038, 2020.

Wakeford, Z. E., Chmielewska, M., Hole, M. J., Howell, J. A., and Jerram, D. A.: Combining thermal imaging with photogrammetry of an active volcano using UAV: an example from Stromboli, Italy, Photogrammetric Record, 34, 168, 445-466, https://doi.org/10.1111/phor.12301, 2019.

Walter, T. R., Ratdomopurbo, A., Subandriyo, N., Aisyah, K., Brotopuspito ,S., Salzer, J., and Lühr, B.: Dome growth and coulée spreading controlled by surface morphology, as determined by pixel offsets in photographs of the 2006 Merapi eruption, J. Volcanol. Geotherm. Res., 261, 121–129, https://doi.org/10.1016/j.jvolgeores.2013.02.004, 2013.

Wang, D., Shao, Q., and Yue, H.: Surveying Wild Animals from Satellites, Manned Aircraft and Unmanned Aerial Systems (UASs): A Review, Remote Sensing, 11, 1308, https://doi.org/10.3390/rs11111308, 2019.

Westfeld, P., Mader, D., and Maas ,H.-G.: Generation of TIR-attributed 3D point clouds from UAV-based thermal imagery, Photogrammetrie–Fernerkundung Geoinformation , 2015, 381–393, https://dx.doi.org/10.1127/1432-8364/2015/0274, 2015.

Westoby, M. J., Brasington, J., Glasser, N. F., Hambrey, M. J., and Reynolds, J. M.: "Structure-from-Motion" photogrammetry: a low-cost, effective tool for geoscience applications, Geomorphology, 179, 300–314. https://doi.org/10.1016/j.geomorph.2012.08.021, 2012.

Yajima, R., Nagatani, K, and Yoshida, K.: Development and field testing of UAV-based sampling devices for obtaining volcanic products," 2014 IEEE International Symposium on Safety, Security, and Rescue Robotics, 1-5, https://doi.org/10.1109/SSRR.2014.7017680, 2014.